(2)

Developing Improved Nuclear Magnetic Resonance Marginal Oscillator Spectrometers for Advanced Teaching Laboratories

CPT Frank P. Willingham
HQDA, MILPERCEN (DAPC-OPA-E)
200 Stovall Street
Alexandria, VA 22332

Final report, 28 October 1988

A thesis submitted to Texas A&M University, College Station, Texas in partial fulfillment of the requirements for the degree of Master of Science (Physics).

SECURITY CLASSIFICATION OF THIS PAGE

REPORT DOCUMENTATION PAGE

Form Approved
OMB No. 0704-0188
Exp. Date: Jun 30, 1986

1a. REPORT SECURITY CLASSIFICATION	1b. RESTRICTIVE MARKINGS
2a. SECURITY CLASSIFICATION AUTHORITY	3. DISTRIBUTION / AVAILABILITY OF REPORT
2b. DECLASSIFICATION / DOWNGRADING SCHEDULE	
4. PERFORMING ORGANIZATION REPORT NUMBER(S) Developing Improved Nuclear Magnetic Resonance Marginal Oscillator Spectrometers for Advanced Teaching Laboratories	5. MONITORING ORGANIZATION REPORT NUMBER(S) Final Report 28 October 1988
6a. NAME OF PERFORMING ORGANIZATION / 6b. OFFICE SYMBOL (If applicable)	7a. NAME OF MONITORING ORGANIZATION FRANK P. WILLINGHAM CPT, IN
6c. ADDRESS (City, State, and ZIP Code)	7b. ADDRESS (City, State, and ZIP Code) 933 Navidad Street Bryan, TX 77801
8a. NAME OF FUNDING / SPONSORING ORGANIZATION / 8b. OFFICE SYMBOL (If applicable)	9. PROCUREMENT INSTRUMENT IDENTIFICATION NUMBER Student, HQDA, MILPERCEN (DAPC-OPA-E) 200 Stovall Street, Alexandria, VA 22332
8c. ADDRESS (City, State, and ZIP Code)	10. SOURCE OF FUNDING NUMBERS PROGRAM ELEMENT NO. / PROJECT NO. / TASK NO. / WORK UNIT ACCESSION NO

11. TITLE (Include Security Classification)
HQDA, MILPERCEN, ATTN:DAPC-OPA-E
200 Stovall Street, Alexandria, VA 22332

12. PERSONAL AUTHOR(S)
28 October 1988

13a. TYPE OF REPORT	13b. TIME COVERED	14. DATE OF REPORT (Year, Month, Day)	15. PAGE COUNT
FINAL	FROM 2 Jun 86 TO 28 Oct 88		56

16. SUPPLEMENTARY NOTATION
Approved for public release; distribution is unlimited.

17. COSATI CODES			18. SUBJECT TERMS (Continue on reverse if necessary and identify by block number)
FIELD	GROUP	SUB-GROUP	Thesis for Texas A&M University. Nuclear Magnetic Resonance; Paramagnetic Resonance; Marginal Oscillator Spectrometer; NMR Spectroscopy

19. ABSTRACT (Continue on reverse if necessary and identify by block number)

Three marginal oscillator circuits are evaluated in their signal-to-noise performance in a complete nuclear magnetic resonance spectrometer. A circuit based on the hybrid Darlington source follower is superior to the other two, a modified Donnally oscillator and an FET cascade oscillator. Also the hybrid Darlington circuit has a voltage gain of 0.95 as compared, respectively, to 0.79 and 0.53 for the other two circuits. A sensitive but easy to understand phase sensitive detector of original design is presented as an integral part of the system, allowing simultaneous observation of the Lorentzian absorption signal and its derivative. Another new development is an external RF injection mode of operation of the marginal oscillators which permits observation of easily saturated NMR lines. Using this system, the variation of proton line widths in water as a function of the concentration of paramagnetic $CuSO_4$ in the water is presented. Also a precise comparison of the gyromagnetic ratio of the F^{19} nucleus to that of the proton yields 0.9409 +/- 0.0007.

20. DISTRIBUTION / AVAILABILITY OF ABSTRACT	21. ABSTRACT SECURITY CLASSIFICATION
☒ UNCLASSIFIED/UNLIMITED ☐ SAME AS RPT. ☐ DTIC USERS	
22a. NAME OF RESPONSIBLE INDIVIDUAL	22b. TELEPHONE (Include Area Code) / 22c. OFFICE SYMBOL

DD FORM 1473, 84 MAR — 83 APR edition may be used until exhausted. All other editions are obsolete.

SECURITY CLASSIFICATION OF THIS PAGE

DEVELOPING IMPROVED NUCLEAR MAGNETIC RESONANCE MARGINAL OSCILLATOR SPECTROMETERS FOR ADVANCED TEACHING LABORATORIES

A Thesis

by

FRANK PHILLIP WILLINGHAM

Submitted to the Office of Graduate Studies of
Texas A&M University
in partial fulfillment of the requirements for the degree of

MASTER OF SCIENCE

December 1988

Major Subject: Physics

DEVELOPING IMPROVED NUCLEAR MAGNETIC RESONANCE MARGINAL OSCILLATOR SPECTROMETERS FOR ADVANCED TEACHING LABORATORIES

A Thesis

by

FRANK PHILLIP WILLINGHAM

Approved as to style and content by:

Nelson M. Duller
(Co-Chair of Committee)

Robert H. Benson
(Co-Chair of Committee)

Robert A. Kenefick
(Member)

Richard L. Arnowitt
(Department Head)

December 1988

ABSTRACT

Developing Improved Nuclear Magnetic Resonance Marginal Oscillator Spectrometers for Advanced Teaching Laboratories. (December 1988)

Frank Phillip Willingham, A.S., Georgia Military College;

B.S., The United States Military Academy

Co-Chairs of Advisory Committee: Dr. Nelson M. Duller
Dr. Robert H. Benson

Three marginal oscillator circuits are evaluated in their signal-to-noise performance in a complete nuclear magnetic resonance spectrometer. A circuit based on the hybrid Darlington source follower is superior to the other two, a modified Donnally oscillator and an FET cascade oscillator. Also the hybrid Darlington circuit has a voltage gain of 0.95 as compared, respectively, to 0.79 and 0.53 for the other two circuits. A sensitive but easy to understand phase sensitive detector of original design is presented as an integral part of the system, allowing simultaneous observation of the Lorentzian absorption signal and its derivative. Another new development is an external RF injection mode of operation of the marginal oscillators which permits observation of easily saturated NMR lines. Using this system, the variation of proton line widths in water as a function of the concentration of paramagnetic $CuSO_4$ in the water is presented. Also a precise comparison of the gyromagnetic ratio of the F^{19} nucleus to that of the proton yields 0.9409 ± 0.0007.

ACKNOWLEDGEMENTS

I extend my heartfelt thanks to Dr. Nelson Duller, for without his help, encouragement and guidance this work would not have come to pass. To Ahmed, Chariar, Jasson, Jim and Henry. Thanks for all your help, understanding and patience. Finally, to my wife Liz, who always had confidence in me, I acknowledge her untiring support and love.

TABLE OF CONTENTS

CHAPTER		Page
I	INTRODUCTION	1
II	CLASSICAL THEORY OF NUCLEAR MAGNETIC RESONANCE ABSORPTION	2
	A Introduction	2
	B Magnetic Resonance Phenomenon	2
	C Nuclear Magnetic Relaxation	8
	D The Bloch Equations	14
	E The RF Susceptibilities and the Saturation Phenomenon	18
III	EXPERIMENTAL APPARATUS	24
	A Introduction	24
	B The Modified Donnally Oscillator	24
	C The Hybrid Darlington Oscillator	27
	D The FET Cascade Oscillator	29
	E The Isolation Stage	29
	F The Audio Amplifier	29
	G The Narrow-Band Amplifier	31
	H The Phase-Sensitive Detector System	32
	I The Phase Shifter	35
	J The RF Injection System	36
IV	EXPERIMENTAL RESULTS	39
	A Introduction	39
	B Signal-to-Noise Measurements	39
	C Proton Resonance Line Widths	40
	D Gyromagnetic Ratio Measurements	43
V	CONCLUSION	46
	REFERENCES	47
	VITA	49

LIST OF TABLES

Table		Page
1	Marginal oscillator signal-to-noise ratio (SNR) measurements.	40
2	Observed absorption line width as a function of molarity.	41
3	Ratio of the fluorine gyromagnetic ratio to that of the proton.	45

LIST OF FIGURES

Figure		Page
1	The relationship between $\vec{B}_{eff}$ in the fixed coordinate system and the rotating coordinate system.	7
2	$\vec{B}_{eff}$ in the rotating coordinate system.	8
3	Spiraling path of precessing tip of magnetization vector $\vec{M}$.	9
4	Beat phenomenon of M_y.	10
5	A pictorial representation of the magnetization $\vec{M}$ fixed in the $Y' - Z'$ plane of the rotating frame.	17
6	Block diagram of experimental apparatus.	25
7	The modified Donnally oscillator circuit.	26
8	The magnet and coil assembly.	27
9	The hybrid Darlington oscillator circuit.	28
10	The FET cascade oscillator circuit.	30
11	The separate audio amplifier circuit.	31
12	The narrow-band amplifier circuit.	32
13	The phase-sensitive detector circuit.	33
14	The differential amplifier circuit.	34
15	The power amplifier circuit.	35
16	The phase shifter circuit.	37
17	The RF injection system.	38
18	Sample calibration plot.	42
19	Representative line width plot.	43

CHAPTER I

INTRODUCTION

Techniques for direct observation of nuclear magnetic resonance (NMR) absorption signals under the constraints of steady state conditions, equivalently slow or "adiabatic" passage through resonance, are classifiable into three general categories: the constant-current oscillator-absorption method first used by Rollins;[1] the marginal oscillator pioneered by Pound and Knight[2] and refined by Robinson;[3] and the bridge method first used by Purcell, Torrey, and Pound[4] and later refined by Grivet, Soutif, and Gabillard.[5] Of these three methods, the marginal oscillator is by far the simplest in regard to frequency adjustment to match the Larmor precession of the nuclei under study. The principal drawback of the original marginal oscillator has always been the inherent difficulty of controlling the level of radio frequency power which excites transitions in the nuclear sample. For students in advanced undergraduate laboratories, who often use the marginal oscillator technique because of its simplicity of design and construction, the problem is further compounded by the use of inexpensive student-built circuits. Though the circuit components normally used are of high quality and the elementary circuits themselves are time-tested, the need for improved sensitivity, stability, ease of use, and signal-to-noise ratio is apparent if the student is to derive optimum results from his handiwork. The plan for the present work included development of a series of marginal oscillators with improved design and performance characteristics. The research presented here also had as a second major objective the design and construction of all associated circuitry for the detection and amplification of the absorption signal for display on an oscilloscope and its first derivative for display on an X-Y recorder.

The format of this thesis is that of the journal *Physical Review B*.

CHAPTER II

CLASSICAL THEORY OF NUCLEAR MAGNETIC RESONANCE ABSORPTION

A. Introduction

A development of the use of rotating coordinate systems to describe the phenomenon of nuclear magnetic resonance and how macroscopic magnetization is manipulated by use of radio frequency (RF) fields is presented here. The analytical results of this discussion are combined with phenomenological descriptions of magnetic relaxation to derive the well known Bloch equations.

The connection between the phenomenological Bloch equations and the RF susceptiblities χ' and χ'' is then developed and some essential theory of nuclear magnetic resonance absorption is presented.

B. Magnetic Resonance Phenomenon

Basic classical dynamics

When a magnetic dipole $\vec{\mu}$ is placed in a magnetic field $\vec{B}$, the result is that a net torque $\vec{\tau}$ is exerted on the magnetic dipole described by the relation

$$\vec{\tau} = \vec{\mu} \times \vec{B} \quad . \tag{1}$$

The energy of a magnetic dipole in a $\vec{B}$-field is given by the expression

$$U_d = -\vec{\mu} \cdot \vec{B} \quad . \tag{2}$$

Also, there is a linear relationship between the magnetic dipole moment $\vec{\mu}$ and the angular momentum $\vec{L}$, with the proportionality constant universally expressed as the *gyromagnetic ratio* γ:

$$\vec{\mu} = g\frac{e}{2m}\vec{L} = \gamma\vec{L} \quad . \tag{3}$$

where g is a constant characteristic of the nuclear species; e is the magnitude of the charge of the proton; m is the mass of the proton; and $\vec{L}$ is the particle's spin angular momentum.

From classical mechanics, the key equation of motion of a dipole $\vec{\mu}$ in the magnetic field $\vec{B}$ is

$$\vec{\tau} = \frac{d\vec{L}}{dt} = \frac{1}{\gamma}\frac{d\vec{\mu}}{dt} \quad . \tag{4}$$

Equating (1) and (4) yields

$$\frac{1}{\gamma}\frac{d\vec{\mu}}{dt} = \vec{\mu} \times \vec{B} \quad , \tag{5}$$

which gives

$$\frac{d\vec{\mu}}{dt} = \vec{\mu} \times \gamma\vec{B} \quad . \tag{6}$$

This equation can be shown to describe also the time variation of the expectation value of the magnetization in the quantum mechanical description, giving then the proper equation of motion of the macroscopic magnetization vector $\vec{M}$, which is discussed and manipulated so often in the present exposition. The net macroscopic magnetization $\vec{M}$ is related to the elementary dipole moment $\vec{\mu}$ by the quantum and statistical mechanical averages of the operator $\vec{\mu}_{op}$ which represents $\vec{\mu}$ in the quantum mechanical formalism. If N is the number of dipoles per unit volume, then $\vec{M} = N\langle\vec{\mu}_{op}\rangle_{ave}$. In this equation, $\vec{M}$ is the effective average of $\vec{\mu}$ per unit volume, and it is this macroscopic vector field whose time variation (exclusive of relaxation effects) is described by equation (6). Relaxation effects to be described later are not included here. It is desirable to proceed with this equation to develop a valid picture of the phenomenon of magnetic resonance of "free spins" (spins not interacting with each other or the lattice). Equation (6) then becomes

$$\frac{d\vec{M}}{dt} = \vec{M} \times \gamma\vec{B} \tag{7}$$

in an inertial frame. It could be useful for some purposes to establish the precise modification of equation (7) when the whole experimental apparatus rotates relative to any inertial frame of reference. This modification will be derived in detail in the next section.

Larmor precession

Consider two Cartesian coordinate systems, one fixed with respect to the laboratory (the laboratory frame of reference) and one which is rotating relative to the laboratory frame with an angular velocity $\vec{\omega}$ (the rotating frame of reference). Projecting the time variation of any vector $\vec{A}$ into a coordinate system rotating at angular velocity $\vec{\omega}$ is done via the relation

$$\left(\frac{d\vec{A}}{dt}\right)_{LAB} = \left(\frac{d\vec{A}}{dt}\right)_{ROT} + \vec{\omega} \times \vec{A} \quad . \tag{8}$$

Thus equation (7) projected into a rotating coordinate system (replace $\vec{A}$ with $\vec{M}$) becomes

$$\begin{aligned}\left(\frac{d\vec{M}}{dt}\right)_{ROT} &= \left(\frac{d\vec{M}}{dt}\right)_{LAB} - \vec{\omega} \times \vec{M} \\ &= \left(\frac{d\vec{M}}{dt}\right)_{LAB} + \vec{M} \times \vec{\omega} \quad ,\end{aligned} \tag{9}$$

which by rearrangement of factors becomes

$$\left(\frac{d\vec{M}}{dt}\right)_{ROT} = \vec{M} \times \gamma \left(\vec{B} + \frac{\vec{\omega}}{\gamma}\right) \quad . \tag{10}$$

Defining the effective magnetic field as

$$\vec{B}_{eff} = \vec{B} - \frac{\vec{\omega}}{\gamma} \tag{11}$$

transforms (10) to precisely the form of (7):

$$\left(\frac{d\vec{M}}{dt}\right)_{ROT} = \vec{M} \times \gamma \vec{B}_{eff} \quad . \tag{12}$$

Fixing the magnetic field $\vec{B}$ along the Z-axis (B_z = constant) and choosing the angular velocity of the rotating frame to make $\vec{B}_{eff} = 0$ yields

$$\vec{\omega} = -\hat{k}\gamma B_z \quad . \tag{13}$$

The important result is that if our rotating coordinate system is chosen to rotate in a "left-handed" manner about the direction of $\vec{B} = \hat{k}B_z$ at the value $\omega = \gamma B_z$.

then the fixed magnetization in the rotating frame is necessarily precessing about the laboratory Z-axis at the angular velocity given by $\vec{\omega} = -\hat{k}\gamma B_z$. This result illustrates what is called *Larmor precession*[6] of the magnetization vector in the laboratory frame of reference.

It is now appropriate to relax the assumption that the laboratory coordinate system (in which the apparatus will be fixed) is not rotating relative to inertial space and in fact assume that it is rotating at a rate denoted by $\vec{\Omega}$ relative to any inertial frame. Using the subscript "I" to denote "as observed in inertial space," we rewrite equation (7):

$$\left(\frac{d\vec{M}}{dt}\right)_I = \vec{M} \times \gamma\vec{B} \quad . \tag{14}$$

Applying the method of (8), gives

$$\left(\frac{d\vec{M}}{dt}\right)_I = \left(\frac{d\vec{M}}{dt}\right)_{LAB} + \vec{\Omega} \times \vec{M} \quad . \tag{15}$$

By the same manipulation as that used to derive equation (10), one finds

$$\left(\frac{d\vec{M}}{dt}\right)_{LAB} = \vec{M} \times \gamma\left(\vec{B} + \frac{\vec{\Omega}}{\gamma}\right) \quad . \tag{16}$$

This expression is quite general and provides the necessary modification of equation (7) to take into account any rotation of the apparatus at angular velocity $\vec{\Omega}$ relative to any inertial frame. Henceforth in all discussions of $\left(\frac{d\vec{M}}{dt}\right)_{LAB}$ it will be proper to include the effects of "absolute rotation" of the laboratory (the apparatus) by simply adding an effective magnetic field $\vec{\Omega}/\gamma$ to the actual field that is applied in the laboratory. (For ordinary laboratory work effects of the rotation of the laboratory tied to the earth are negligible.)

Effects of a weak transverse rotating field

With the addition (to the fixed magnetic field $\hat{k}B_z$) of a magnetic field of amplitude $\vec{B}_1$ which rotates in a left-handed sense at angular frequency ω_0 about the Z-axis of the laboratory frame

$$B_1(i\cos\omega_0 t - j\sin\omega_0 t) \tag{17}$$

the total $\vec{B}$-field is

$$\vec{B} = B_1(\hat{i}\cos\omega_o t - \hat{j}\sin\omega_o t) + \hat{k}B_z \quad . \tag{18}$$

In general, B_1 will be of much smaller amplitude than B_z in experiments of interest here. Establishing $\vec{\omega} = -\hat{k}\omega = -\hat{k}'\omega$, the equation of motion becomes

$$\left(\frac{d\vec{M}}{dt}\right)_{ROT} = \vec{M} \times \gamma\left[\hat{i}B_1\cos\omega_o t - \hat{j}B_1\sin\omega_o t + \hat{k}\left(B_z - \frac{\omega}{\gamma}\right)\right] \quad . \tag{19}$$

Letting $\omega = \omega_o$ allows the rotating magnetic field in the lab coordinate system to be stationary in the rotating coordinate system. Additionally, depending only on an initial condition of arbitrarily defining the rotating X-axis, or X' as it will be denoted, as the axis in the transverse plane of the rotating system which is parallel to $\vec{B}_1$, changes equation (19) to

$$\left(\frac{d\vec{M}}{dt}\right)_{ROT} = \vec{M} \times \gamma\left[\hat{i}'B_1 + \hat{k}'\left(B_z - \frac{\omega}{\gamma}\right)\right] \quad . \tag{20}$$

Figure 1 shows the two coordinate systems as defined above with the primed system rotating at ωt with respect to the unprimed laboratory system in a *left-handed* sense about $\vec{B}_z$.

Again, from the method of equation (12), one recognizes the effective magnetic field in the rotating frame as

$$\vec{B}_{eff} = \hat{i}'\, B_1 + \hat{k}'\left(B_z - \frac{\omega}{\gamma}\right) \quad . \tag{21}$$

thus reducing (20) to the simple form

$$\left(\frac{d\vec{M}}{dt}\right)_{ROT} = \vec{M} \times \gamma\vec{B}_{eff} \quad . \tag{22}$$

Clearly, from an examination of the two components of $\vec{B}_{eff}$ in (21), when the Z' component is zero, the X' component ($\hat{i}'B_1$) is the only field component remaining in the rotating frame and

$$\omega_z = \gamma B_z \quad . \tag{23}$$

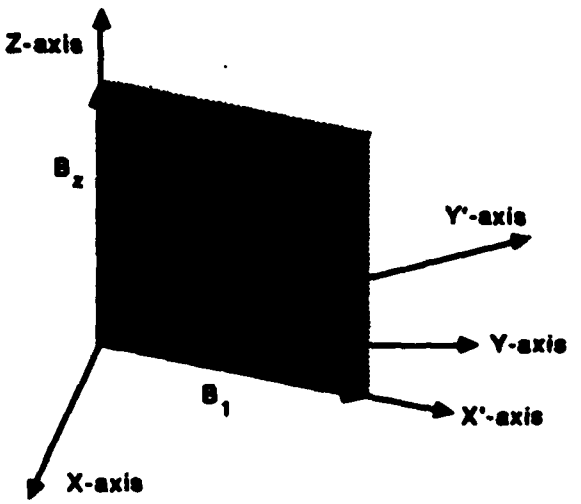

Figure 1. The relationship between $\vec{B}_{eff}$ in the fixed coordinate system and the rotating coordinate system. The net magnetic field is made up of two components, the fixed component $\vec{B}_z$ and the rotating component $\vec{B}_1$. The conventional relationships between the two coordinate systems is shown for positive γ. The field $\vec{B}_1$ is drawn here relatively much larger than it normally is for the sake of clarity.

This gives the frequency of exact resonance and corresponds to the frequency of the rotating field $\vec{B}_1$. Essential to this derivation is the assumption that the field $\vec{B}_z$ is precisely uniform throughout the sample of nuclear dipoles, a condition which can only be approximated in the laboratory. Figure 2 shows explicitly that, as the magnitude of $|\omega/\gamma|$ approaches the value of $|\vec{B}_z|$, the value of $\vec{B}_{eff}$ approaches just the small transverse component $\vec{B}_1$. Thus, the condition of magnetic resonance is realized when the magnetization $\vec{M}$ "sees" only the fixed vector $\vec{B}_1$ in the rotating frame and thus precesses about it rather slowly as compared with the angular rate of the rotating frame about the laboratory Z–axis. If, for example, the rotating field is turned on at resonance at time $t = 0$ with the initial magnetization along the Z–axis, then this magnetization vector will precess in the $Y' - Z'$ plane in the rotating frame, executing a spiraling motion (down and back up again repeatedly) as viewed in the laboratory frame, as is shown in Figure 3. An inductive pickoff coil with its axis

in the laboratory transverse plane will receive an RF signal modulated as shown in Figure 4. Such a signal or variations of it can be readily observed by use of simple apparatus with appropriate choices of experimental parameters.

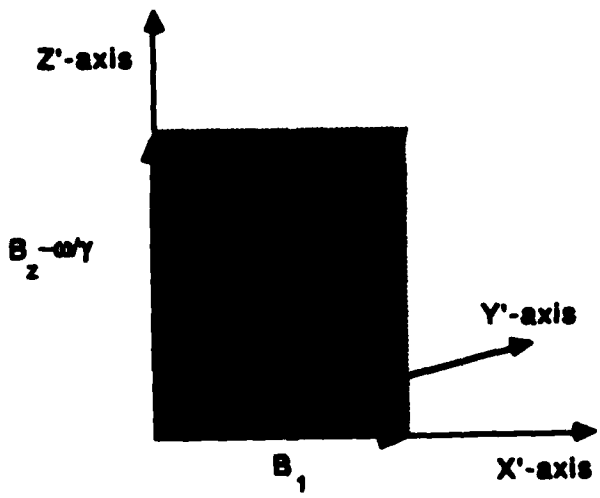

Figure 2. $\vec{B}_{eff}$ in the rotating coordinate system. The effective magnetic field $\vec{B}_{eff}$ in the rotating frame of reference moves with $\vec{B}_1$. Again, $\vec{B}_1$ is drawn relatively much larger than is normally used in NMR experiments for illustration purposes. Notice that $\vec{B}_z$ is reduced by $(\omega/\gamma)\hat{k}$ in the rotating frame of reference.

C. Nuclear Magnetic Relaxation

Introduction

When nuclear magnetic resonance was first observed in bulk matter, Bloch[7] introduced two phenomenological relaxation times, T_1 and T_2, which are of great usefulness in describing the effects of the atomic and nuclear environment of nuclear magnetic dipoles.

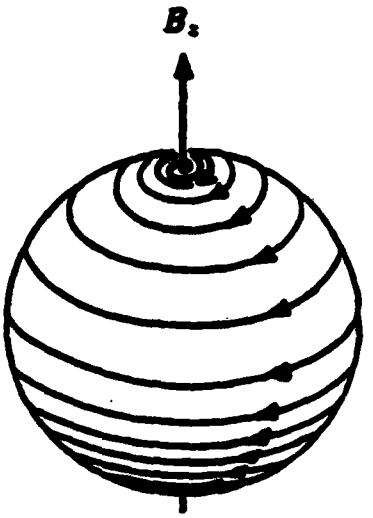

Figure 3. **Spiraling path of precessing tip of magnetization vector $\vec{M}$. The illustration shows the path of the tip of the magnetization vector $\vec{M}$ at magnetic resonance assuming that $\vec{M}$ is initially along $\vec{B}_z$ as it would be in thermal equilibrium.**

The Boltzmann factor

It is not possible with the apparatus in this experiment to observe the effects of a single nuclear magnetic dipole in our samples, which have volumes on the order of a cubic centimeter. It is essential, therefore, to make use of statistical mechanics in describing the bulk effects of spin 1/2 particles (e.g. protons). At equilibrium (relaxed state), the value of net magnetization is observed to be

$$\begin{aligned} \vec{M} &= \chi \vec{H} \\ &= \frac{\chi_o}{\mu_o} \vec{B} \quad , \end{aligned} \tag{24}$$

where

$\chi_o \equiv$ the static magnetic susceptibility.

This is a result of a fraction of the dipoles being aligned, a condition which depends on the absolute temperature of the lattice, the strength of $\vec{H}$, and the type of nuclear

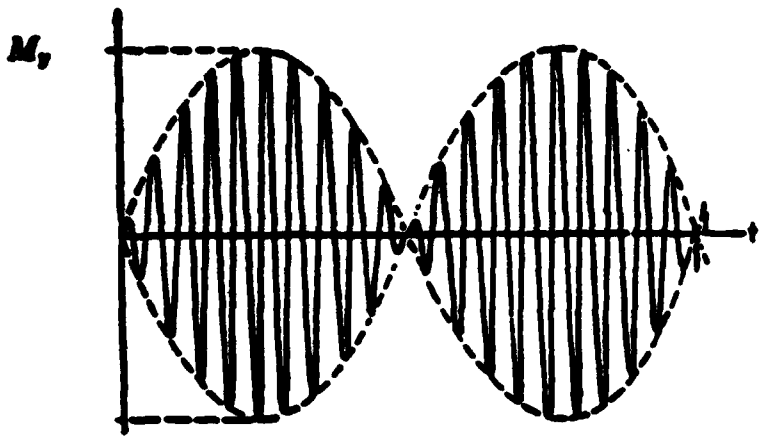

Figure 4. Beat phenomenon of M_y. Illustrated above is a component of $\vec{M}$ (e.g., M_y) at magnetic resonance transverse to $\vec{B}_z$ in the laboratory coordinate system. A transverse pickoff coil will have a voltage induced at the Larmor frequency.

species (characterized by γ). From statistical mechanics for spin 1/2 systems, the ratio of the population of the two spin states $m = +1/2$ and $m = -1/2$ is

$$\frac{N(+1/2)}{N(-1/2)} = \exp\left[\frac{U_p(-1/2) - U_p(+1/2)}{kT}\right] \quad . \tag{25}$$

where

$U_p(-1/2)$ = dipole energy of spin-up proton (aligned with $\vec{B}$),

$U_p(-1/2)$ = dipole energy of spin-down proton (anti-aligned with $\vec{B}$),

k = Boltzmann constant.

and T = absolute temperature on the Kelvin scale.

The term

$$\exp\left[\frac{U_p(-1/2) - U_p(-1/2)}{kT}\right]$$

is known as the *Boltzmann factor*.[8] Among other important uses, it predicts the equilibrium fractional excess of aligned dipoles producing a net magnetization along

the static magnetic field which depends on the absolute temperature of the lattice and the energy difference between aligned and anti-aligned nuclei. By inspection of the Boltzmann factor it is clear that increasing equilibrium magnetization will result by lowering the absolute temperature or strengthening the static magnetic field. For example, with protons at room temperature in a magnetic field of 10,000 gauss, the energy difference in the numerator of the exponential of the Boltzmann factor is about 3×10^{-19} ergs and the value of kT is about 4×10^{-14} ergs. These numbers lead to a net magnetization along the magnetic field which is produced by a very small fractional excess alignment of nuclei: for every million nuclei in the sample, the net excess number aligned along the field is about four. With the same protons at room temperature in a field of 25 gauss, for every 100 million nuclei in the sample, the net excess number aligned along the field is only about one.

The longitudinal relaxation time, T_1

In a liquid macroscopic sample of nuclear dipoles at thermal equilibrium there is no preferred orientation of the dipoles when there is no externally applied magnetic field. As discussed earlier, when a magnetic field is applied each magnetic dipole experiences a torque $\vec{\tau} = \vec{\mu} \times \vec{B}$ causing the dipoles to try to align along the applied $\vec{B}$. The alignment torques compete with local disorienting thermal effects. Since the energy of each dipole in $\vec{B}$ is given by $U_d = -\vec{\mu} \cdot \vec{B}$, any alignment of dipoles reduces the energy of the dipole sample (i.e., it "cools" the system) and some mechanism for conserving energy is required for a complete description. It has been shown in detail by many workers that the "reservoir" to which the spin systems give up their energy is the "lattice" of the bulk material. (See Abragam[9], Bloembergen[10], and Pake.[11]) The *lattice* has become the comprehensive term for all internal structure and atomic content of the bulk matter which surrounds the dipoles. The electromagnetic interaction (for liquids, due largely to Brownian motion) between the spins and the lattice which causes energy transfers is universally called "the spin-lattice interaction." Bloch[7] made the assumption that any paramagnetic ensemble of dipoles in a magnetic field would "relax" exponentially with a time constant T_1, which is determined by the

atomic structure of the bulk matter, to an equilibrium value yielding a net magnetization along the applied magnetic field given by $\vec{M}_o = (\chi_o/\mu_o)\vec{B}$. Mathematically, this relaxation phenomenon can be expressed as

$$\frac{dM_z}{dt} = \frac{M_o - M_z}{T_1} \quad , \tag{26}$$

where the laboratory Z-axis is taken along $\vec{B}$. T_1 is known as "the longitudinal relaxation time" and always involves energy transfer to or from the lattice.

The transverse relaxation time, T_2

There are several useful and interesting ways to cause a net magnetization $\vec{M}$ in the direction of $\vec{B}$ to rotate into a plane perpendicular to $\vec{B}$, thus producing what is often called a "transverse magnetization." As has been shown above, this transverse vector will execute Larmor precession about $\vec{B}$. However, the number of individual dipoles that contribute to this transverse $\vec{M}$ will be reduced in time by two effects:

(1) relaxation toward alignment along $\vec{B}_z$ with the longitudinal relaxation time T_1; and

(2) a transverse dephasing which "fans out" the dipoles by mutual interaction between them and by inhomogeneities of the externally applied $\vec{B}$-field.

The transverse interactions do not involve exchange of energy with the lattice but rather conserve magnetic energy because they effectively exchange spin directions between pairs of dipoles and cause random fluctuations in the local magnetic field. in the process interrupting the orderly coherent precession of the magnetization about the magnetic field and introducing a "dephasing" effect among the dipoles. This dephasing of the transverse component of $\vec{M}$ combined with the longitudinal relaxation described above has been shown to cause an exponential decay of transverse magnetization with a time constant T_2, "the transverse relaxation time," first introduced by Bloch.[7] The relaxation of the two transverse components of magnetization thus is described by the equation

$$\frac{dM_{x,y}}{dt} = -\frac{M_{x,y}}{T_2} \quad . \tag{27}$$

Equations (26) and (27) have played an enormously important role in representing relaxation phenomena in the well known Bloch equations derived below.

It is important to note that $T_2 \leq T_1$ in general as a result of the fact that the attenuation of transverse magnetization is caused by longitudinal relaxation (which controls T_1) as well as by purely transverse "dephasing effects." The Brownian motion in many liquids and vapors contributes to a great reduction in the average internal magnetic field. Fluctuations in the field at a given nuclear site due to frequent electromagnetic collisions average very nearly to zero gauss over an interval of one Larmor precession period. Thus in such liquids and vapors, T_1 and T_2 are very nearly equal.

Instrument T_2 and magnetic field homogeneity requirements

No matter how carefully one designs and constructs magnets, it is physically impossible to produce a perfectly uniform external magnetic field throughout the entire volume of any real sample of nuclear dipoles. For this reason, dipoles at different positions in a given sample will, in general, precess at different rates. How different these rates are depends directly on the homogeneity of the magnetic field. Inhomogeneities in fields produced by such practical configurations as ordinary solenoids and even Helmholtz coils can cause very pronounced dephasing of a transverse component of magnetization, in many instances providing the dominant cause of decay. In experiments involving passage through resonance in which, for example, NMR absorption "lines" (or peaks) are observed, such field inhomogeneity dephasing causes a decrease in the effective T_2 which is qualitatively indistinguishable from the effects of the intrinsic T_2. By convention, this additional contribution is accounted for by "instrument T_2" denoted by T_2^i such that

$$T_2^i = (\gamma \triangle B)^{-1} \quad . \tag{28}$$

where $\triangle B$ is an appropriate measure of the variation of the $\vec{B}$–field over the sample volume (e.g., the rms deviation of the field from its average value). Unless one uses special pulse–field "echo" techniques such as the spin–echo or rotary phase–switch

methods,[12] the result will be a loss of transverse magnetization governed by a decay time

$$\frac{1}{T_2^*} = \frac{1}{T_2} + \frac{1}{T_2'} \quad , \tag{29}$$

where T_2^* is the decay time observed in NMR absorption (and dispersion) experiments and causes a broadening of the observed line widths. Precision of the field and frequency values which characterize an NMR absorption peak thus puts stringent requirements on the homogeneity of the applied magnetic field over the volume of an NMR dipole sample.

D. The Bloch Equations

In equation (7) we have the time rate of change of the total nuclear magnetization caused by the torque on the dipoles by the magnetic field $\vec{B}$:

$$\frac{d\vec{M}}{dt} = \vec{M} \times \gamma \vec{B} \quad . \tag{30}$$

The Bloch equations describe the time rate of change of the three Cartesian components of the nuclear magnetization when the spin sample is subjected to a very specific field:

$$\vec{B} = i2B_1 \cos \omega t - \hat{k} B_z \quad . \tag{31}$$

In experimental situations of interest here, B_1 will be in the range from a few milli-gauss to $\sim$ 1.0 gauss, always much smaller than B_z. In actual laboratory apparatus, the transverse field, $i2B_1 \cos \omega t$, is produced by what is commonly called (in Bloch's nuclear induction method) the *transmitter coil* (usually a single solenoid) arranged with its axis parallel to the laboratory X-axis. The NMR equipment used in this work combines the transmitter coil and *receiver coil* into simply one tuned inductor containing the sample of nuclear dipoles.

A technique which is useful in simplifying later calculations is to resolve the linearly polarized component $i2B_1 \cos \omega t$ into two circularly polarized fields

$$i2B_1 \cos \omega t = (iB_1 \cos \omega t - jB_1 \sin \omega t) + (iB_1 \cos \omega t - jB_1 \sin \omega t) \quad . \tag{32}$$

The first expression in parentheses describes a "right-handed" rotation of a field of magnitude B_1, and the second set of parentheses contains the corresponding "left-handed" expression. Only the left-handed circularly polarized $\vec{B}_1$-field will be effective in nuclear magnetic resonance experiments because only this component can "follow" the left-handed Larmor precession of most nuclei (with positive gyromagnetic ratios, γ). For small values of B_1, the right-handed component can be ignored (incoherence averages it to zero from the viewpoint of any precessing nucleus), and so in the context of the Bloch theory describing nuclear magnetic resonance we express $\vec{B}$ in the laboratory frame as

$$\vec{B} = iB_1 \cos \omega t - jB_1 \sin \omega t + \hat{k}B_z \quad . \tag{33}$$

This expression for $\vec{B}$ in the laboratory is readily transformed to the same magnetic field as viewed in the rotating frame which is rotating about the $\hat{k} = \hat{k}'$ direction in a left-handed sense at angular frequency ω

$$\vec{B} = i'B_1 + \hat{k}'\left(B_z - \frac{\omega}{\gamma}\right) \equiv \vec{B}_{eff} \quad . \tag{34}$$

So now the equation describing the time rate of change in $\vec{M}$ in the rotating frame is (momentarily ignoring relaxation terms):

$$\begin{aligned}
\left(\frac{d\vec{M}}{dt}\right)_{ROT} &= \vec{M} \times \gamma \vec{B}_{eff} \\
&= \vec{M} \times \gamma \left[i'B_1 + \hat{k}'\left(B_z - \frac{\omega}{\gamma}\right)\right] \\
&= \left(i'M_{x'} - j'M_{y'} - \hat{k}'M_{z'}\right) \times \gamma \left[i'B_1 - \hat{k}'\left(B_z - \frac{\omega}{\gamma}\right)\right] \\
&= i'M_{y'}\gamma\left(B_z - \frac{\omega}{\gamma}\right) - j'\left[M_{z'}\gamma B_1 - M_{x'}\gamma\left(B_z - \frac{\omega}{\gamma}\right)\right] \\
&\qquad - \hat{k}'M_{y'}\gamma B_1 \quad .
\end{aligned} \tag{35}$$

Thus the combination of the magnetic resonance condition and the relaxation phenomena yields the three Bloch equations expressed in a rotating frame (rotating

at the frequency ω of the $\vec{B}_1$–field in the laboratory reference frame):

$$\begin{aligned}
\frac{dM_{x'}}{dt} &= \gamma M_{y'}\left(B_z - \frac{\omega}{\gamma}\right) - \frac{M_{x'}}{T_2} \\
\frac{dM_{y'}}{dt} &= \gamma\left[M_{z'}B_1 - M_{x'}\left(B_z - \frac{\omega}{\gamma}\right) - \frac{M_{y'}}{T_2}\right] \\
\frac{dM_{z'}}{dt} &= -\gamma M_{y'}B_1 - \frac{M_{z'} - M_{o'}}{T_1} \quad .
\end{aligned} \tag{36}$$

After a period of time which allows relaxation effects to occur, the time derivatives of the three magnetization components will vanish. This leaves three linear equations with solution

$$M_{x'} = \frac{(\omega_o - \omega)\gamma B_1 T_2{}^2 M_o}{1 + (\omega_o - \omega)^2 T_2{}^2 + \gamma^2 B_1{}^2 T_1 T_2} \tag{37}$$

$$M_{y'} = \frac{\gamma B_1 T_2 M_o}{1 + (\omega_o - \omega)^2 T_2{}^2 + \gamma^2 B_1{}^2 T_1 T_2} \tag{38}$$

$$M_{z'} = \frac{\left[1 + (\omega_o - \omega)T_2{}^2\right] M_o}{1 + (\omega_o - \omega)^2 T_2{}^2 + \gamma^2 B_1{}^2 T_1 T_2} \quad . \tag{39}$$

The above components of $\vec{M}$ are fixed along their respective axes in the coordinate system rotating at frequency ω in a left–handed sense with respect to the $X - Y - Z$ laboratory frame. Thus it is a simple matter to write the steady state solution as viewed in the laboratory:

$$\begin{aligned}
M_x(t) &= M_{x'}\cos\omega t + M_{y'}\sin\omega t \\
M_y(t) &= -M_{x'}\sin\omega t - M_{y'}\cos\omega t \\
M_z(t) &= M_{z'}(t) \quad .
\end{aligned} \tag{40}$$

The solutions presented here demonstrate the driven nature of the transverse components under the influence of the magnetic field imposed.

Figure 5 depicts the physical situation which prevails at resonance. A steady state value of magnetization is fixed in the rotating frame (rotating at rate ω_o), and this fixed magnetization has a transverse component which, as it rotates, will induce an EMF in a "pickoff coil." This coil acts as a receiver of the NMR signal. Such an arrangement with a separate "transmitter coil" to impose the oscillating (effectively rotating) magnetic field, $\vec{B}_1$, was used by Bloch in his pioneer "nuclear induction" NMR

experiments using bulk matter.[7] The nuclear induction method thus uses "crossed coils" with their axes both perpendicular to the strong, steady field, $\vec{B}_z$. E. M. Purcell, *et al.* simultaneously (and independently) developed the essential equivalent of the "marginal oscillator" technique of detecting NMR signals.[4] His method combines the transmitter and receiver function in a single coil which surrounds the bulk sample of nuclear dipoles. A net absorption shows up as a transiently spoiled "Q" of the coil as the resonant condition is traversed. The net absorption results from two essential conditions:

(a) the slight excess of nuclear spins in the lower energy state over the number in the higher energy state: and

(b) the loss of energy from the spin system to the "lattice" (all surrounding material) only from spins in the higher energy state.

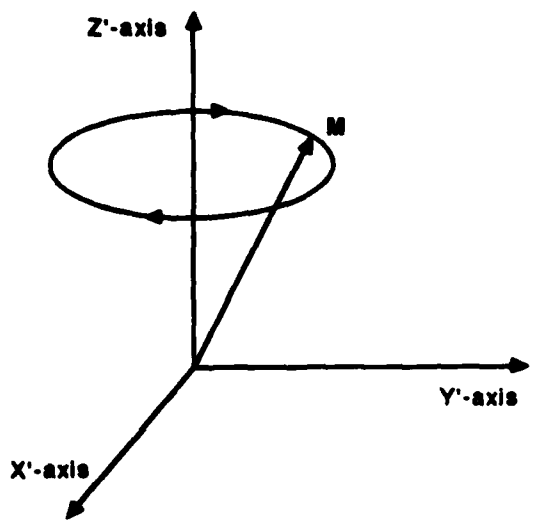

Figure 5. A pictorial representation of the magnetization $\vec{M}$ fixed in the $Y' - Z'$ plane of the rotating frame. The indicated "left-handed" rotation about the Z'-axis causes the Y' component of $\vec{M}$ to induce an EMF in a pickoff coil with axis lying in the transverse laboratory plane.

This latter energy leak prevents the perpetual alternate loss-and-gain cycle which prevails with "free spins." And it is for this reason, among others, that in water samples some addition of a paramagnetic salt to reduce T_1 can enhance the signal observed in a marginal oscillator over that which can be seen with relatively pure water.

E. The RF Susceptibilities and the Saturation Phenomenon

In almost all experiments involving the small magnetic field denoted by $\vec{B}_1$ in all of the preceding analyses, the production of $\vec{B}_1$ is done by causing a purely sinusoidal radio-frequency current to flow through a solenoid at a frequency denoted by ω. The fact that the solenoid produces an alternating linear field along its axis which is decomposed into two (oppositely) circularly polarized fields of amplitude B_1 means that in the laboratory the actual RF field is given by $\hat{\imath}2B_1\cos\omega t$, with unit vector $\hat{\imath}$ along the X-direction in the laboratory because that has been the arbitrary choice of the coil orientation.

The magnetization $\vec{M}$ which is produced by response of the nuclear sample to the excitation provided by $\hat{\imath}2B_1\cos\omega t$ is the basis for the *defining equations* yielding the RF susceptibilities traditionally denoted as χ' and χ'' in the laboratory frame of reference:

$$M_x(t) = \frac{1}{\mu_c}(\chi' 2B_1\cos\omega t + \chi'' 2B_1\sin\omega t) \quad . \tag{41}$$

The defining equation allows $M_x(t)$ to have a component exactly in phase with the driving field $H(t) = 2(B_1/\mu_c)\cos\omega t$ and also (as it turns out, essential) a component precisely 90° out-of-phase with the driving field $H(t)$.

Now to get explicit expressions for χ' and χ'' in terms of the previous work on the components of M_x and M_y (and $M_{x'}$, $M_{y'}$) produced by the RF excitation $2B_1\cos\omega t$ in the sample coil, the terms of equation (40) are compared with those of equation (41): results of this comparison are:

$$M_{x'} = 2\frac{B_1}{\mu_c}\chi' \qquad \text{and} \qquad M_{y'} = 2\frac{B_1}{\mu_c}\chi'' \quad . \tag{42}$$

These two equations then give the two RF susceptibility formulas. First,

$$\begin{aligned}\chi' &= \frac{1}{2}\frac{\mu_o}{B_1}M_{x'} \\ &= \frac{1/2(\omega_o-\omega)\gamma T_2^2(\mu_o M_o)}{1+(\omega_o-\omega)^2T_2^2+\gamma^2B_1^2T_1T_2} \quad .\end{aligned} \tag{43}$$

Then, using the following relationships,

$$\omega_o = \gamma B_z \qquad \text{and} \qquad M_o = \chi_o\frac{B_z}{\mu_o} \quad , \tag{44}$$

the combination of which yields

$$\mu_o M_o = \chi_o B_z = \chi_o\frac{\omega_o}{\gamma} \quad , \tag{45}$$

one conventional form of χ' is given by

$$\chi' = \frac{1}{2}\omega_o\chi_o T_2\frac{T_2(\omega_o-\omega)}{1+(\omega_o-\omega)^2T_2^2+\gamma^2B_1^2T_1T_2} \quad . \tag{46}$$

And similarly,

$$\begin{aligned}\chi'' &= \frac{1}{2}\frac{\mu_o}{B_1}M_{y'} \\ &= \frac{1}{2}\frac{\mu_o}{B_1}\frac{\gamma B_1T_2M_o}{1+(\omega_o-\omega)^2T_2^2+\gamma^2B_1^2T_1T_2} \\ &= \frac{1}{2}\omega_o\chi_oT_2\frac{1}{1+(\omega_o-\omega)^2T_2^2+\gamma^2B_1^2T_1T_2} \quad .\end{aligned} \tag{47}$$

For reasons which will be developed later, it turns out that the factor χ'' is directly and exclusively responsible for the *absorption NMR line* that can be observed with the proper equipment. The factor χ' is responsible for the *NMR dispersion signal* and does not involve absorption of energy from the excitation/receiver coil which radiates the enclosed nuclear sample by the $\vec{B}_1$-field.

Now to show explicitly the phenomenon known as *saturation broadening* of the NMR absorption line, it is necessary to anticipate a fact that will be demonstrated later, namely that the absorption line is essentially represented by $M_{y'}$:

$$M_{y'} = \frac{\gamma B_1T_2M_o}{1+(\omega_o-\omega)^2T_2^2+\gamma^2B_1^2T_1T_2} \quad . \tag{48}$$

It is useful in this context to write out the standard normalized Lorentz function in terms of parameters which have direct bearing on the NMR absorption phenomenon:

$$f_{T_2}(\omega) = \frac{T_2}{\pi} \frac{1}{1 + (\omega_o - \omega)^2 T_2^2} \quad . \tag{49}$$

At this point it is important to note two items:

(1) **the half-width at half-maximum of the signal is given by $1/(T_2)$, and**

(2) **the very important term $\gamma^2 B_1^2 T_1 T_2$ does not appear in the standard Lorentz function.**

The purpose in this development is to show explicitly that

$$M_{y'} = \frac{\pi \gamma B_1 M_o}{(1 + \gamma^2 B_1^2 T_1 T_2)^{1/2}} f_{T_2'}(\omega) \quad , \tag{50}$$

in which

$$\frac{1}{T_2'} = \frac{1}{T_2}(1 + \gamma^2 B_1^2 T_1 T_2)^{1/2} \quad , \tag{51}$$

thus demonstrating that when the *saturation parameter*. $S_p \equiv \gamma^2 B_1^2 T_1 T_2$, grows to values that compare with 1.0 or larger the line is "saturation broadened."

The method of showing the expression immediately above is a simple (but algebraically long) brute force identity problem. The expression

$$\frac{1}{T_2'} = \frac{1}{T_2}(1 + \gamma^2 B_1^2 T_1 T_2)^{1/2} \tag{52}$$

is injected into the formula for $M_{y'}$ (See equation (50)) by use of the following manipulation. First divide the denominator by the factor

$$(1 + \gamma^2 B_1^2 T_1 T_2) \tag{53}$$

and multiply the numerator by

$$(1 + \gamma^2 B_1^2 T_1 T_2)^{-1} \tag{54}$$

in the form

$$\frac{(1 + \gamma^2 B_1^2 T_1 T_2)^{-1/2}}{(1 + \gamma^2 B_1^2 T_1 T_2)^{1/2}} \quad . \tag{55}$$

Thus,

$$M_{y'} = \frac{\gamma B_1 M_o T_2 (1+\gamma^2 B_1{}^2 T_1 T_2)^{-1/2}}{(1+\gamma^2 B_1{}^2 T_1 T_2)^{1/2}} \left(\frac{1+\gamma^2 B_1{}^2 T_1 T_2}{1+(\omega_o-\omega)^2 T_2{}^2 + \gamma^2 B_1{}^2 T_1 T_2} \right)$$
$$= \frac{\gamma B_1 M_o T_2}{(1+\gamma^2 B_1{}^2 T_1 T_2)^{1/2}} \left(\frac{(1+\gamma^2 B_1{}^2 T_1 T_2)^{1/2}}{1+(\omega_o-\omega)^2 T_2{}^2 + \gamma^2 B_1{}^2 T_1 T_2} \right) \qquad (56)$$
$$= \frac{\pi \gamma B_1 M_o}{(1+\gamma^2 B_1{}^2 T_1 T_2)^{1/2}} \frac{T_2'}{\pi} \left(\frac{1}{1+(\omega_o-\omega)^2 T_2'{}^2} \right) \quad ,$$

in which

$$T_2' = \frac{T_2}{(1+\gamma^2 B_1{}^2 T_1 T_2)^{1/2}} \quad . \qquad (57)$$

Making use of equation (49), the normalized Lorentz function, $M_{y'}$ becomes

$$M_{y'} = \frac{\pi \gamma B_1 M_o}{(1+\gamma^2 B_1{}^2 T_1 T_2)^{1/2}} f_{T_2'}(\omega) \quad . \qquad (58)$$

Thus the "saturation broadening" of the absorption line has the dependence on B_1 given by

$$\frac{1}{T_2'} = \frac{1}{T_2}(1+\gamma^2 B_1{}^2 T_1 T_2)^{1/2} \quad . \qquad (59)$$

It is now useful to show that even though the absorption line is broadened by the factor shown in the preceding analysis, the maximum value of the important "signal generating" magnetization $M_{y'}$ (yet to be demonstrated) is produced when $\gamma^2 B_1{}^2 T_1 T_2 = 1.0$ at resonance. To do this the derivative of $M_{y'}$ is taken with respect to B_1 as follows:

$$\frac{dM_{y'}}{dB_1} = \frac{(\gamma B_1 T_2 M_o)(2\gamma^2 B_1 T_1 T_2) - (1+(\omega_o-\omega)^2 T_2{}^2 + \gamma^2 B_1{}^2 T_1 T_2)\gamma T_2 M_o}{(1+(\omega_o-\omega)^2 T_2{}^2 - \gamma^2 B_1{}^2 T_1 T_2)^2} \quad . \qquad (60)$$

Then at resonance $\omega = \omega_o$ and

$$\left(\frac{dM_{y'}}{dB_1} \right)_{\omega=\omega_o} = 0 \qquad (61)$$

when

$$\gamma B_1 T_2 M_o (2\gamma^2 B_1 T_1 T_2) - (1-\gamma^2 B_1{}^2 T_1 T_2)\gamma T_2 M_o = 0 \quad . \qquad (62)$$

Canceling common factors $\gamma T_2 M_o$ leaves

$$2\gamma^2 B_1{}^2 T_1 T_2 - 1 - \gamma^2 B_1{}^2 T_1 T_2 = 0 \quad . \qquad (63)$$

which is equivalent to requiring that

$$\gamma^2 B_1^2 T_1 T_2 = 1.0 \quad . \tag{64}$$

It is then evident that the largest absorption signal is achieved when the saturation parameter is unity. Above that the saturation effect reduces the signal by reducing the difference between spin–up and spin–down nuclei in the sample, whereas below it the excitation effect of the oscillating field of amplitude B_1 is less effective in causing transitions.

It is now time to discuss the long delayed but strongly motivated development of why $M_{y'}$ and therefore the RF susceptibility χ'' are exclusively responsible for the observed NMR absorption line. It is first important to notice that at exact resonance $M_{x'} = 0$ and $M_{y'}$ is at its maximum value. So at resonance, only $M_{y'}$ can induce the signal EMF in the receiver coil. The signal generated by $M_{y'}$ as it rotates at angular velocity ω_o in the laboratory $X - Y$ plane is proportional to $\omega_o M_{y'}$, which is proportional in turn to the rate of flux change in the receiver coil:

$$\omega_o M_{y'} = \frac{\omega_o \gamma B_1 T_2 M_o}{1 + \gamma^2 B_1^2 T_1 T_2} \tag{65}$$

at resonance. Since $M_{y'}$ and χ'' are directly proportional to each other, it is now evident that χ'' is the "absorption" component of the RF susceptibility.

In this context the question may naturally arise as to what physical role χ' plays in the resonance phenomenon we are discussing, and, further, what is the difference between χ'' and χ'? This question is probably most conveniently answered by defining the *complex susceptibility* as

$$\chi = \chi' - j\chi'' \quad . \tag{66}$$

With this seemingly arbitrary definition, equation (41) can be rewritten in complex form:

$$\begin{aligned} \mu_o M_x(t) &= \mathrm{Re}\{2B_1 \chi e^{j\omega t}\} \\ &= \mathrm{Re}\{2B_1(\chi' - j\chi'')(\cos\omega t + j\sin\omega t)\} \\ &= \mathrm{Re}\{2B_1(\chi'\cos\omega t + \chi''\sin\omega t) + j2B_1(\chi'\sin\omega t - \chi''\cos\omega t)\} \\ &= 2B_1\chi'\cos\omega t + 2B_1\chi''\sin\omega t \quad . \end{aligned} \tag{67}$$

Now with the complex susceptibility we can see what effect a nuclear sample inside a coil has on the parameters of the coil. If the inductance of the coil with only vacuum (or air) inside it is called L_o, then when a substance with a susceptibility χ is put inside the coil, the inductance is changed as follows:

$$L = L_o(1 + \chi) \quad . \tag{68}$$

Since any real coil has resistance (ordinary ohmic resistance), which we will call R_o, then the impedance of the coil at frequency ω is given by

$$\begin{aligned} Z &= j\omega L + R_o \\ &= j\omega L_o(1 + \chi' - j\chi'') + R_o \\ &= j\omega L_o(1 + \chi') + (R_o + \omega L_o \chi'') \quad . \end{aligned} \tag{69}$$

So the real part of the RF susceptibility χ' changes the inductance of the coil and the imaginary part, χ'', modifies the resistance of the coil. For reasons that are rooted in the nomenclature of early modern physics, χ' is called the *dispersion* component of χ. It now becomes abundantly clear why χ'' is the *absorption* term in χ.

CHAPTER III

EXPERIMENTAL APPARATUS

A. Introduction

The principal items of equipment developed in this project are three different marginal oscillators, all constructed and tested to measure the only truly important figure of merit for such devices used in NMR measurements: signal–to–noise ratio. All oscillators were coupled to the same NMR detection apparatus, developed especially for this thesis. The oscillator outputs were fed in parallel to an ordinary amplitude modulation detector (AM detector) and a phase–sensitive detector of original design for this work. In the studies of signal–to–noise the signals for various NMR samples could then be viewed simultaneously as data were collected. Figure 6 illustrates the general block diagram of the experiment. In order to facilitate a better understanding of how these components are designed and used in this project each is discussed briefly below.

B. The Modified Donnally Oscillator

The first of the oscillators worked with is the simplest. It is a modern adaptation of a transistor emitter follower oscillator first presented by Donnally and Sanders.[13] It has been modified to operate with an FET as the active element with other modern components included. Subsequently this version of the oscillator will be referred to as the *modified Donnally* oscillator. The other two oscillators are refinements of the modified Donnally oscillator and will be discussed in subsequent sections of this thesis.

A detailed circuit of the modified Donnally oscillator is given in Figure 7. In the diagram it is clear that a fraction of the output at the source of the FET is fed back through a capacitive reactive path to the resonant tank circuit to maintain oscillation. The connection to the stacked capacitors (C_2) in the feedback path is equivalent to feeding current directly from the FET source to a tap on the tank coil.

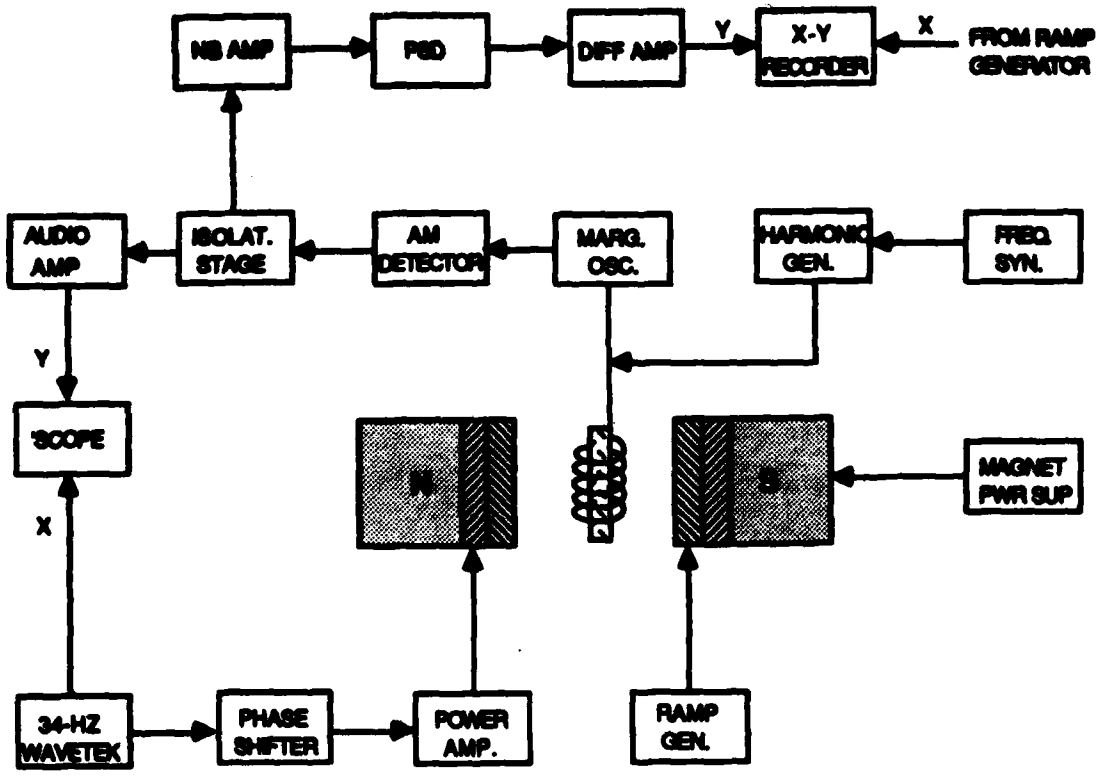

Figure 6. Block diagram of experimental apparatus.

As shown in Figure 8 the tank coil contains the NMR sample and is mounted between the poles of a standard teaching laboratory magnet. The functions of the additional coils labeled *ramp coil* and *wobbling coil* will be described later.

To provide a basis for comparison of gain of the source follower of the Donnally oscillator with that of more sophisticated source followers (e.g., the Darlington circuit), the voltage gain at 16.0 MHz of the simple FET source follower was measured and found to be 0.53. Also various temporal (and somewhat subjective) measures were made of the stability of the modified Donnally oscillator in extreme NMR operating conditions.

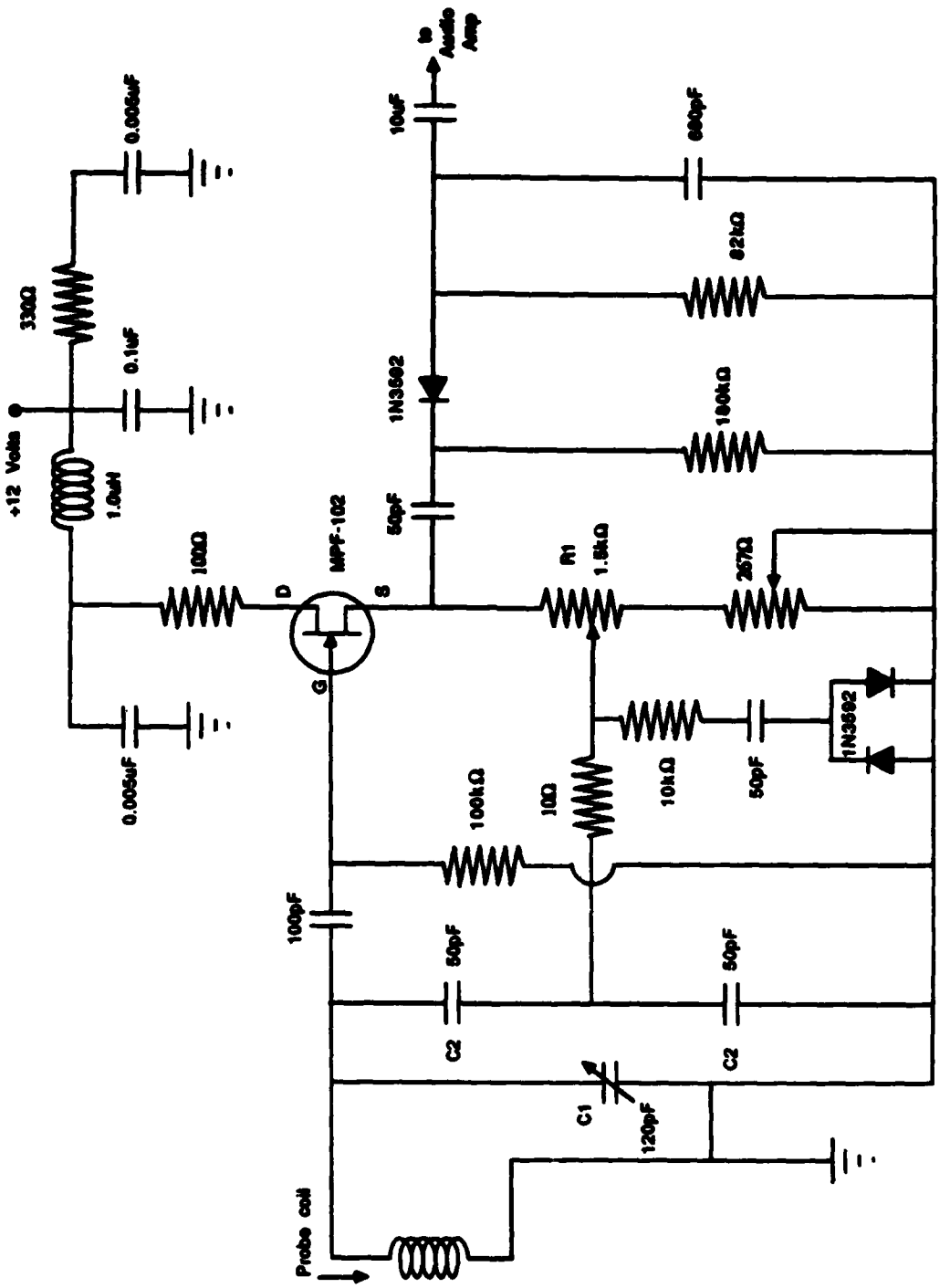

Figure 7. The modified Donnally oscillator circuit.

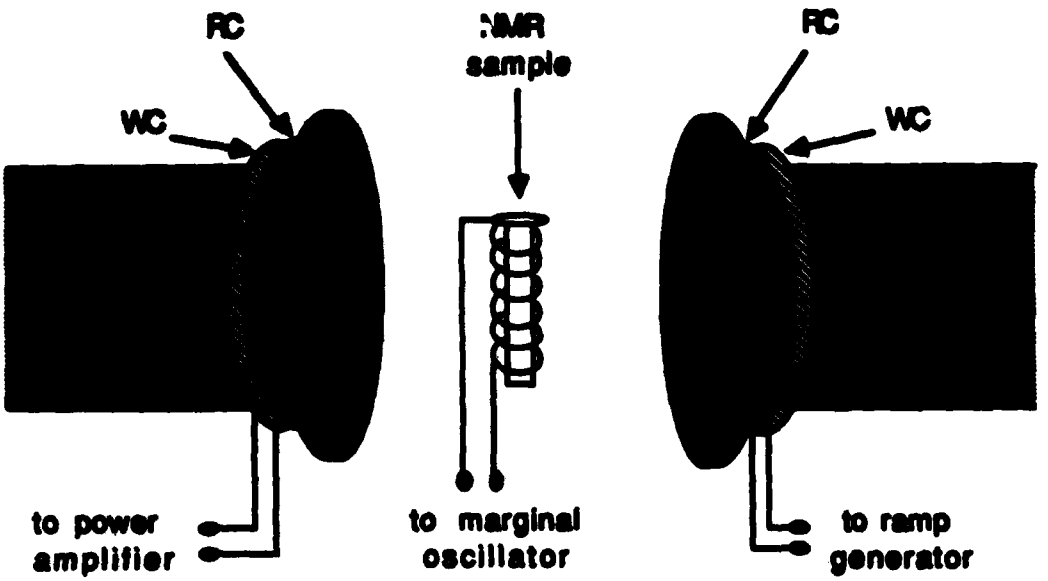

Figure 8. The magnet and coil assembly. The ramp coil (RC in diagram) slowly and linearly changes the field between the pole faces to sweep through the full width of the resonance. The wobbling coil (WC in the diagram) produces a relatively small AC component of the field between the pole faces to generate the derivative signal for the phase sensitive detector.

C. The Hybrid Darlington Oscillator

The effort to explore for better gain and stability of the marginal oscillator component of the NMR system led to the Darlington circuit. Because the FET provides high input impedance at its gate, the Darlington circuit ultimately chosen for this work is a *hybrid* in the sense that the input element is an FET and the support element is a good high-frequency bipolar transistor. It was in this context that the second marginal oscillator, now called the *hybrid Darlington*, was developed.

The bootstrapping provided by capacitors (C_3), as illustrated in Figure 9, reduces the rolloff of gain with increasing signal frequency by alleviating the effects of load and junction capacitance. The hybrid Darlington, as tested, exhibited a voltage gain of 0.95 with no observable phase shift at 16.0 MHz.

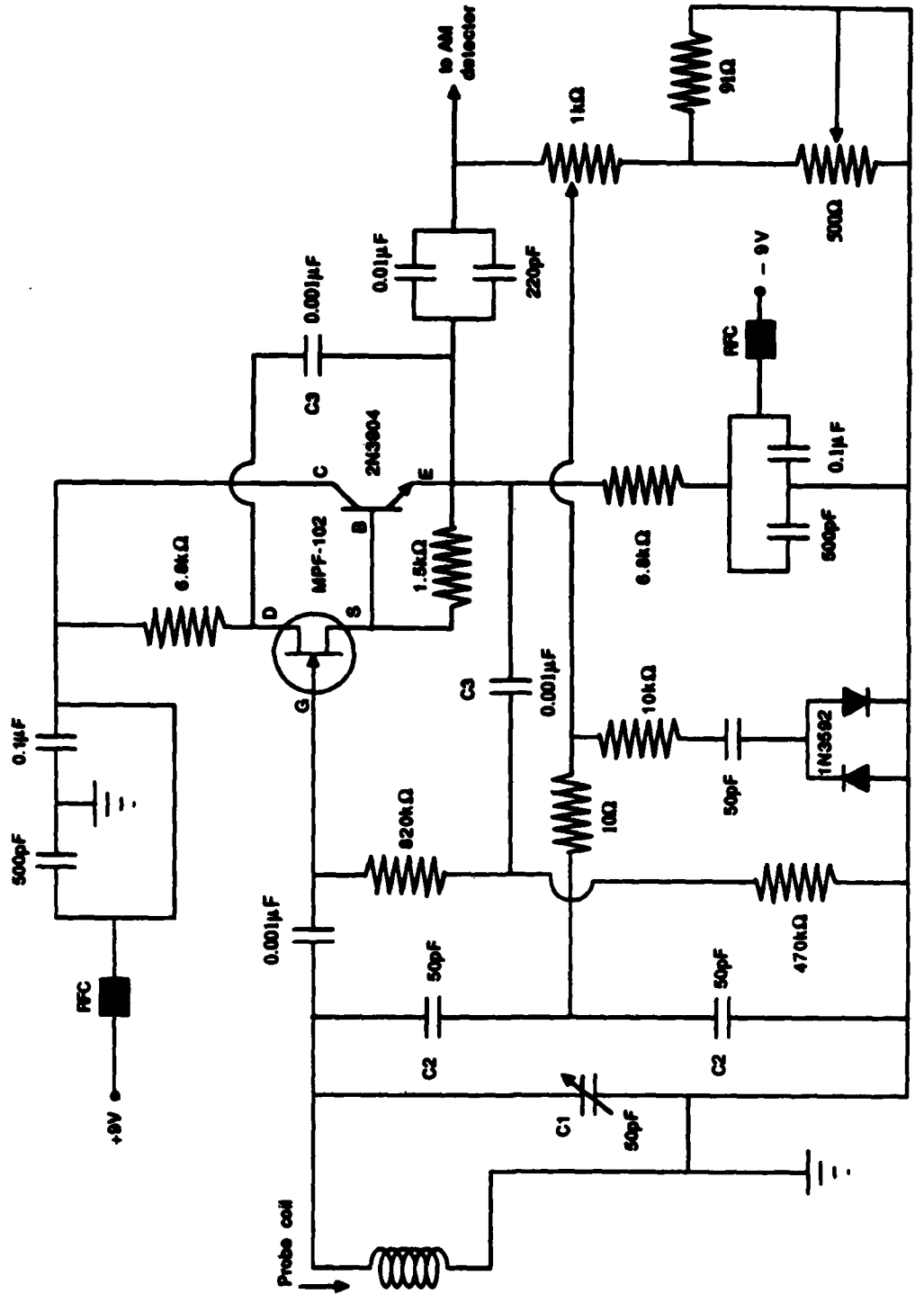

Figure 9. The hybrid Darlington oscillator circuit.

D. The FET Cascade Oscillator

The FET cascade circuit is distinguished from other source followers by replacing the conventional resistor below the source with an active FET constant-current element as shown in Figure 10. This constant current connection of the FET has typically several hundred thousand ohms of AC impedance but allows current to flow through it with rather small effective DC resistance. Following the lead of oscilloscope manufacturers, the FET cascade circuit was experimented with to exploit its potential as the ultimate source follower.

Various combinations of FET's with quality up to and including "matched" components manufactured expressly for oscilloscopes, were tested with disappointing results. The reliable MPF-102 was finally selected for the FET after its use in the cascade circuit was observed to produce a voltage amplification of 0.79 with no observable phase shift at radio frequencies.

E. The Isolation Stage

As stated previously, the oscillator modules simultaneously operate in an absorption display mode and an absorption derivative display mode. To facilitate the dual display mode of operation a hybrid Darlington source follower is used to isolate the output of the marginal oscillator module from the display circuitry. The high input impedance of the source follower prevents the dual display circuitries from loading the marginal oscillator output, allowing the audio signal to be input simultaneously to the audio amplifier and to the narrow band amplifier as illustrated in Figure 6. The hybrid Darlington source follower operates flawlessly at audio frequencies with a voltage amplification of 1.0 and no phase shift.

F. The Audio Amplifier

An audio amplifier is included on the chassis with the modified Donnally oscillator but appears as a separate module for the hybrid Darlington and FET cascade oscillators to avoid further duplication of effort and equipment. The two audio amplifiers are virtually identical with the exception of a variable gain control (R_2), in

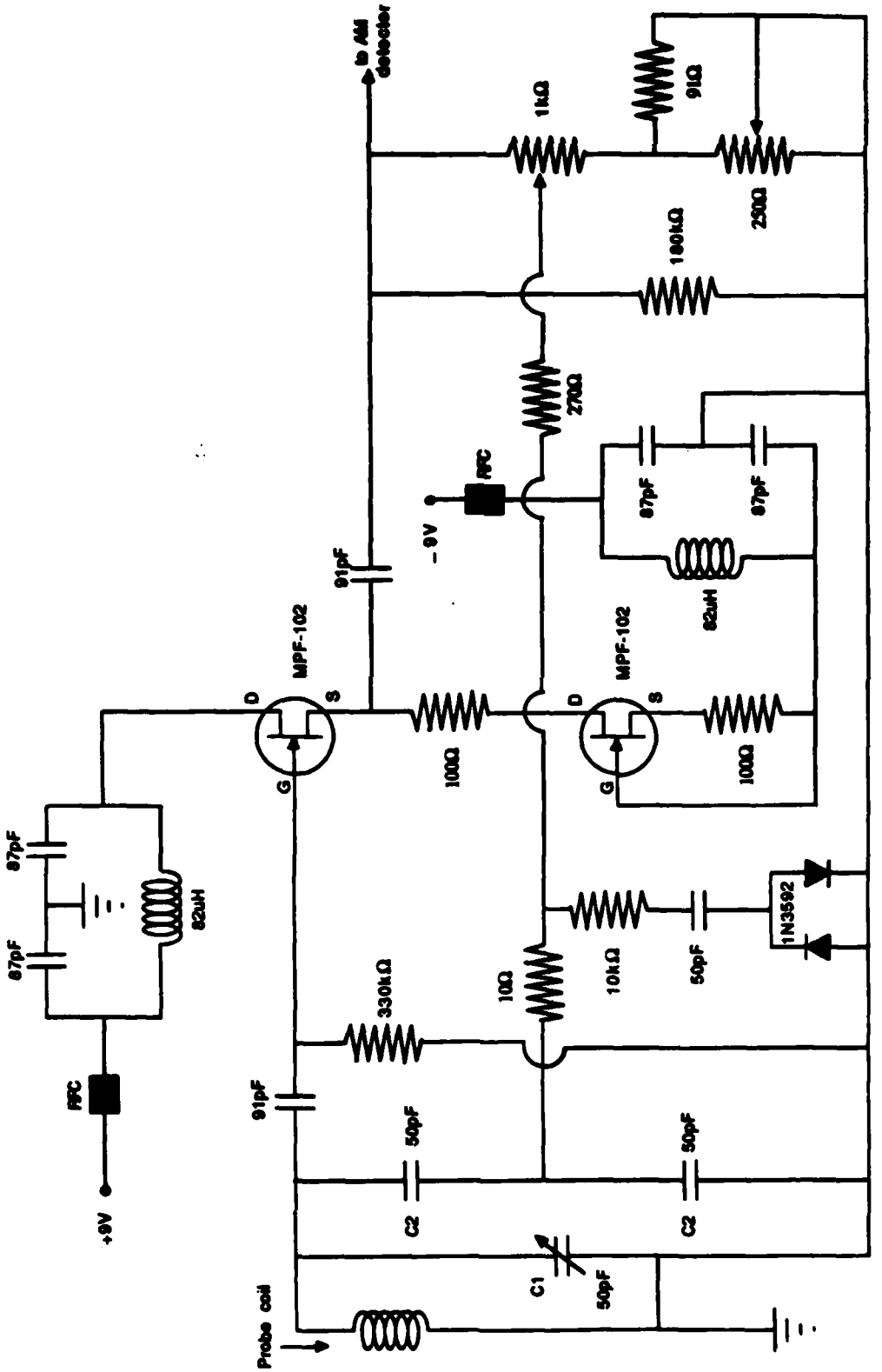

Figure 10. The FET cascade oscillator circuit.

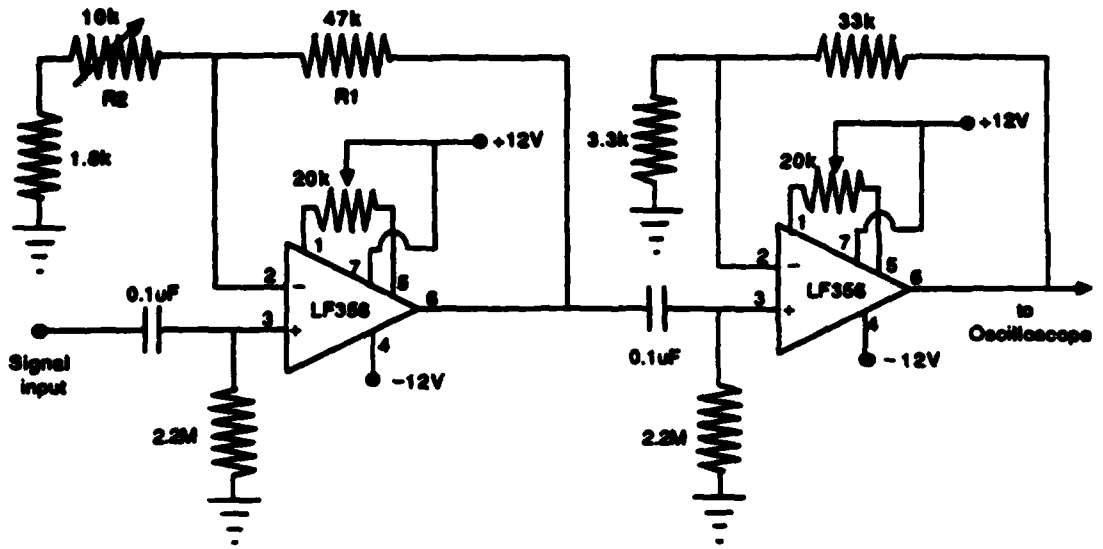

Figure 11. The separate audio amplifier circuit.

the first stage of the separate amplifier module as illustrated in Figure 11. With the gain control the separate amplifier exhibits an overall voltage gain of 52–261. The audio amplifiers are among the few components of the system that utilize integrated circuitry instead of discrete components.

G. The Narrow-Band Amplifier

NMR samples that are easily saturated require low RF levels if their resonance signals are to be observed. Consequently, the desired signal is often smaller than the spurious noise. To extract the NMR signal from the noise, a phase-sensitive detection method is often utilized. Narrow-band amplification of the audio signal is the first effective step of this detection method.

The narrow-band amplifier improves the signal-to-noise ratio of the NMR signal by capitalizing on a tuned amplifier's characteristic of enhancing signals within a narrow band of frequencies, the amplifier "bandpass," while attenuating signals falling

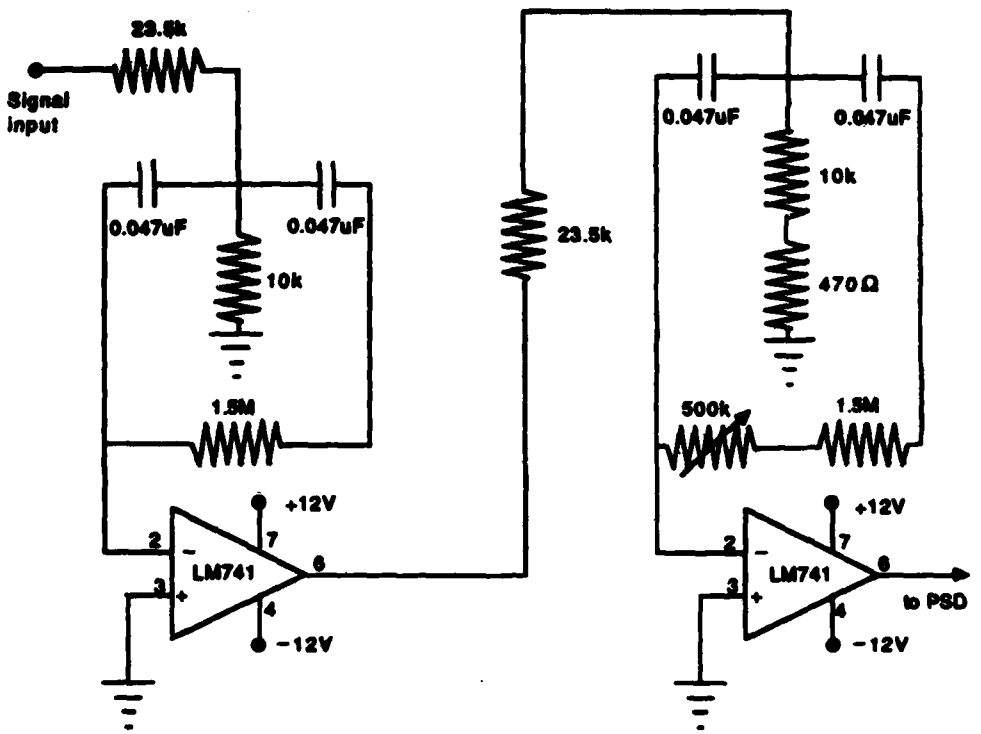

Figure 12. The narrow-band amplifier circuit.

outside this band. In this project, the signal frequency is determined by the frequency of the modulation of the primary magnetic field, $\vec{B}_z$.

As can be seen in Figure 8, the modulation of $\vec{B}_z$ is accomplished by the use of the Helmholtz coils labeled *wobbling coils* that are being driven by a frequency generator operating at 34 Hz. The narrow-band amplifier in Figure 12 therefore is designed for a central frequency of 34 Hz. Judicious selection of components gives the amplifier a voltage gain of 1000 and a bandwidth of 5.5 Hz.

H. The Phase-Sensitive Detector System

The design of the phase-sensitive detector (PSD) employed in this project was intentionally made as simple as could be conceived. Since all PSD's are merely syn-

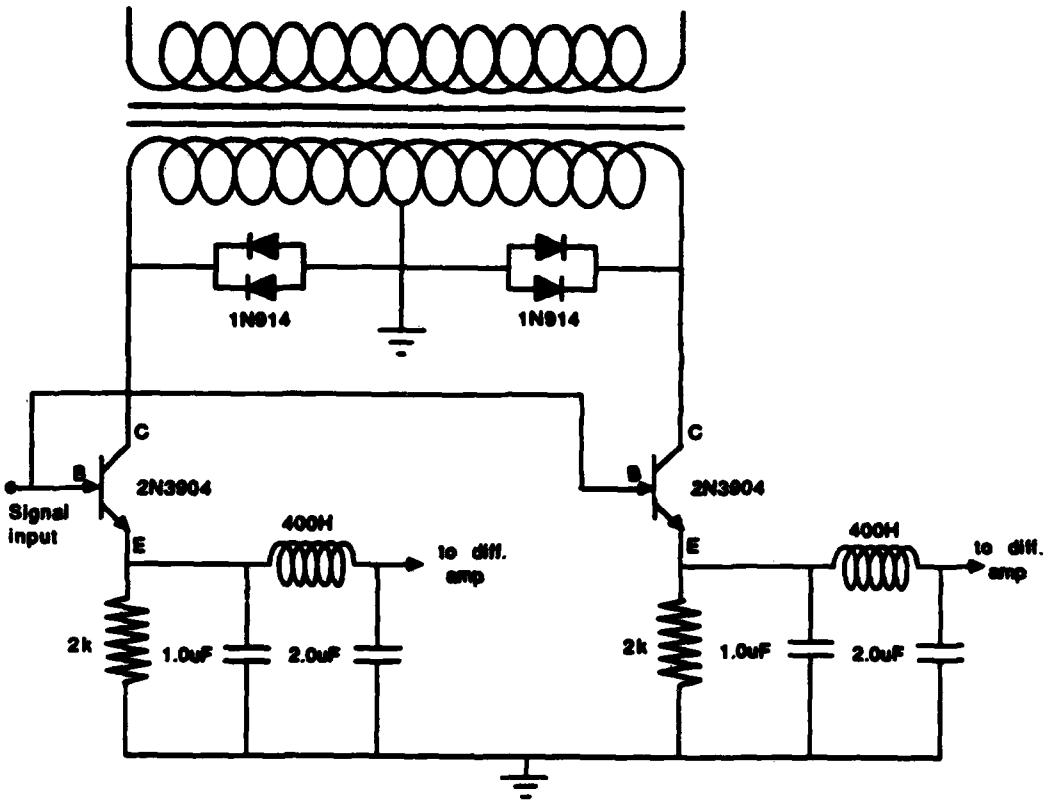

Figure 13. The phase-sensitive detector circuit.

chronous switches in essence, the detector in this experiment was designed to demonstrate the switching function as explicitly as possible. Thus, as is shown in Figure 13, two transistors are alternately *enabled* and *disabled* in a complementary manner by use of a center-tapped transformer driven by a power source which is perfectly coherent with the signal to be demodulated. The actual signal comes from the narrow-band amplifier, which in turn is driven by the response of the NMR sample (through the marginal oscillator) to the 34-Hz wobbling field. The small and carefully controlled amplitude of the wobbling field ensures that the NMR response is proportional to the derivative of the Lorentzian NMR absorption curve. Coherence of the power applied to the PSD with the NMR signal is assured by using a common source of 34-Hz voltage. As shown in Figure 13 the transistors have their bases (input terminals for the PSD) connected together. On the other hand, the two emitters put charge on

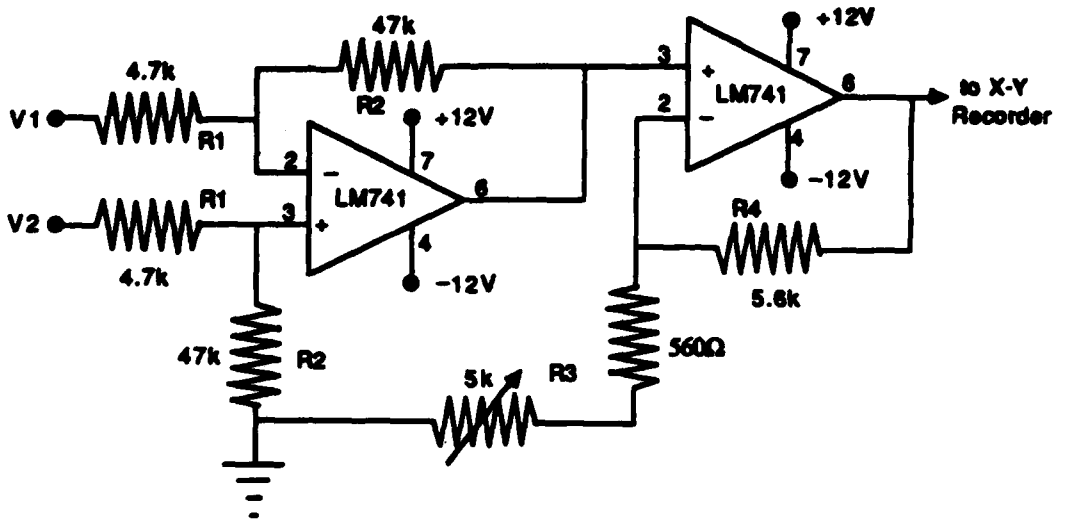

Figure 14. The differential amplifier circuit.

independent integrating capacitors. Thus the actual output of the PSD is the difference between the voltages on these two integrating circuits. Then the differential amplifier shown in Figure 14 is used to amplify this DC potential difference. It should be noted that the PSD can operate with only one of the integrating circuits thereby giving half-wave demodulation instead of full-wave demodulation.

With the equipment described above and with the NMR sample immersed in a $\vec{B}_z$-field at some particular value which lies within the Lorentzian absorption curve limits, the output signal has an amplitude proportional to the slope at one point on the Lorentzian form. By slowly and linearly varying the *ramp field*, which is simply adding to or subtracting from the $\vec{B}_z$-field, the output of the differential amplifier slowly traces out the first derivative of the entire Lorentzian absorption line if ramp excursion is sufficiently large. In all the experiments in this project, such a ramp field was applied using a Wavetek set at approximately 0.003 Hz.

Even though the wobbling field is of small amplitude, a power amplifier is required to drive the wobbling field coils since the Wavetek 34-Hz voltage source is

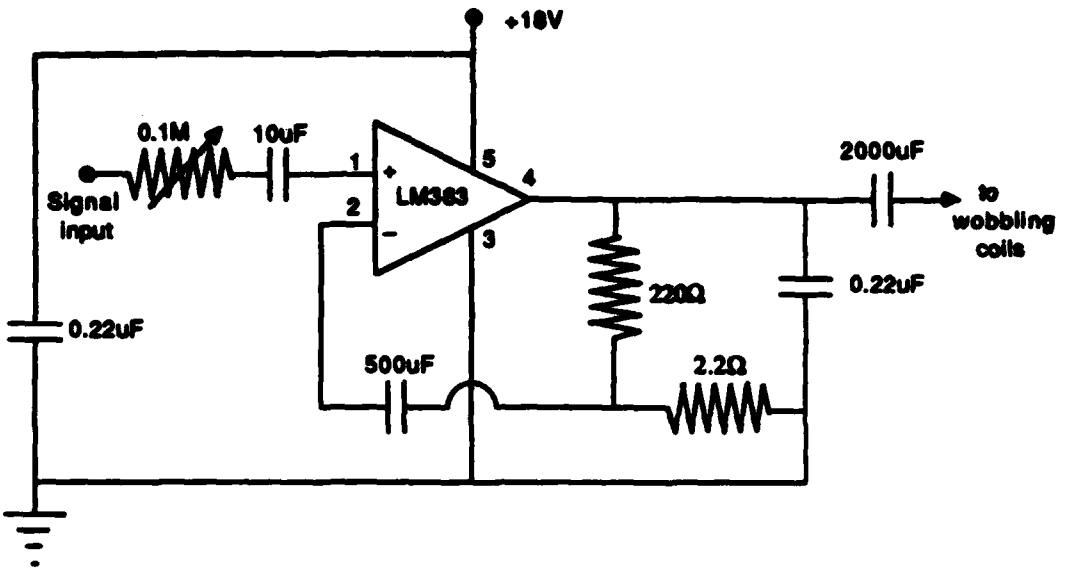

Figure 15. The power amplifier circuit.

entirely inadequate for this purpose. The wobbling field power amplifier is shown in Figure 15.

I. The Phase Shifter

The required coherence between the NMR signal into the PSD and the AC power to the transformer which is an integral part of the PSD is discussed in the preceding description. It now becomes necessary to recognize explicitly that the proper phase between these two AC voltages is also absolutely essential for the proper functioning of the PSD.

To illustrate this point with separate examples of relative phases which give maximum signal amplitudes and null signals, respectively, consider first the ideal phase relation to produce maximum signal amplitudes. If the incoming signal from the narrow-band amplifier on the bases of the two transistors is precisely in phase with the voltage applied to the collector of the transistor on the left in Figure 13, then

this transistor is enabled when the signal is positive. Consequently, during the other half of each cycle, the transistor on the right in Figure 13 is enabled when the signal is negative. This set of circumstances clearly leads to enhanced positive differential voltage of left emitter relative to right emitter. When the ramp proceeds to the other shoulder of the Lorentzian line, the relative phase of signal and collector voltages changes by 180°, so that the differential voltage reverses polarity — i.e., positive voltage of right emitter relative to left emitter. This change in polarity explains the overall appearance of the derivative signal.

An example of a phase relation between the incoming signal and the AC on the two collectors (in the PSD) which leads to a null signal (i.e., no difference in voltage between the two emitters) is simply described by having the input signal 90° out of phase with the signal on the two collectors. In this circumstance the two transistors each spend one-half of their enabled periods with an *average* voltage of zero on their bases with the consequence that the differential output voltage is zero. This zero is conspicuously present in the very center of each derivative signal when the ramp passes through the peak of the Lorentzian.

The phase shifter circuit is shown in Figure 16. This circuit can produce a phase shift close to 180° with no change in amplitude.

J. The RF Injection System

In an experiment which will be described in more detail later, a sample containing both protons and fluorine (F^{19}) is used to compare the gyromagnetic ratios of these two nuclei in precisely the same magnetic field. The sample chosen was trifluorobenzene, each molecule of which contains three protons and three fluorine nuclei. As the experiment progressed the detection of the proton resonance was found to be routine with the marginal oscillator set at a reasonably low and sustainable level of RF in the tank coil. However, hours of searching for the fluorine resonance signal in the proper frequency range were fruitless. The only logical reason for this failure to observe the resonance seemed to be that this particular molecular environment yields such a narrow fluorine line that the RF level successful for protons was completely

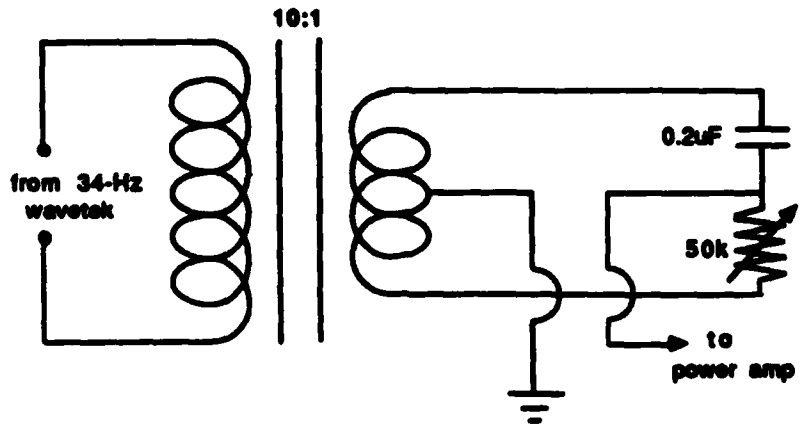

Figure 16. The phase shifter circuit. The output to the power amplifier will change phase through a range close to 180° without change in amplitude.

saturating the fluorine resonance rendering it unobservable. It thus appeared that a much lower RF level in the tank coil should be tried. Many repeated attempts to operate the oscillator at its extreme lowest level of RF were frustrating because of continual interruption of oscillation after just a very few seconds of this low-level adjustment.

At this time a new turn of events not only made the observation of the fluorine resonance signal possible but also helped provide an example of the general character of saturation phenomena and signal optimization as was discussed in Chapter II. The breakthrough was the discovery that a low RF level in the oscillator tank is readily maintained by adjusting the marginal oscillator just below the point of self-sustained oscillation and by then injecting RF power from a stable external oscillator. In this mode of operation the external source is very loosely coupled to the RF tank and serves the purpose of continually shock exciting the marginal oscillator to give continuous very low level RF in the NMR sample. One is tempted to consider the oscillator to be actually a high-Q amplifier, but such an idea is refuted by the fact that

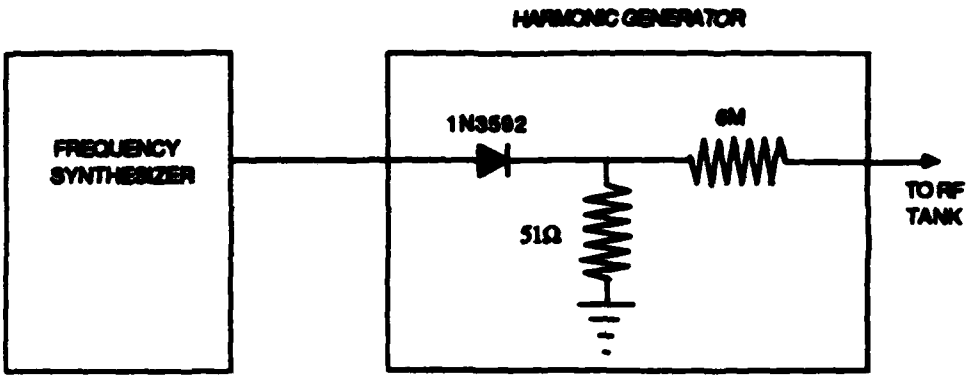

Figure 17. The RF injection system.

beats between the tuned oscillator and the external RF source appear conspicuously on a monitoring oscilloscope.

The RF injection system used is a very stable frequency synthesizer coupled through a silicon diode harmonic generator to get the required frequency of RF power near 15.0 MHz. (The upper limit of the range of the synthesizer alone is 11.0 MHz.) This system is displayed in essential detail in Figure 17.

CHAPTER IV

EXPERIMENTAL RESULTS

A. Introduction

Observation of the resonance absorption signal and of the absorption derivative signal was achieved through application of the theory discussed in Chapter II along with careful measurements using the apparatus discussed in Chapter III. The signal–to–noise ratios of the absorption signal and its derivative provide the primary basis of comparison of the three marginal oscillators constructed for this thesis. The maximum amplitude of the resonance signal occurs when the saturation parameter, S_p, is unity (i.e. $\gamma B_1{}^2 T_1 T_2 = 1$). (See page 21.) For S_p slightly greater than unity, the saturation effect reduces the signal amplitude but increases the stability of the marginal oscillator. Protons were selected as the NMR sample species for signal–to–noise measurements because samples are readily available in which one can easily avoid saturation of the proton line by RF fields produced conveniently in marginal oscillator tank coils. The marginal oscillators were therefore adjusted to provide optimum absorption signal amplitude and stability by using proton samples and by increasing the positive feedback to the tank coil such that S_p was slightly greater than unity.

B. Signal–to–Noise Measurements

Table 1 contains the signal–to–noise measurements taken for the three oscillators utilizing different proton environments, RF coils, frequencies of oscillation, and display modes. The results obtained with the phase–sensitive detection mode of operation are illustrative of the effectiveness of even the simplest home–made phase–sensitive detectors.

These results on the signal–to–noise ratio show that the hybrid Darlington oscillator consistently outperforms the other two oscillators tested. At this time it

Table 1. Marginal oscillator signal-to-noise ratio (SNR) measurements. Signal-to-noise was measured as the signal voltage (peak-to-peak) to the noise voltage (maximum peak-to-peak).

Oscillator	Sample	Absorption SNR	Derivative SNR
modified Donnally	glycerin	10.55 to 1	121.59 to 1
hybrid Darlington	glycerin	24.89 to 1	216.00 to 1
FET cascade	glycerin	5.63 to 1	22.60 to 1
modified Donnally	mineral oil	24.97 to 1	115.56 to 1
hybrid Darlington	mineral oil	33.67 to 1	227.00 to 1
FET cascade	mineral oil	13.03 to 1	40.16 to 1

remains a serious puzzle why the FET cascade oscillator operates so poorly. This lack of performance will be the subject of an investigation entirely separate from the present work. The FET cascade oscillator is henceforth not considered for physical measurements which are to be described in this thesis. Also the hybrid Darlington circuit was chosen over the modified Donnally oscillator for concentrated efforts in two experiments: measurements of proton resonance line widths in NMR samples with broadly varying concentrations of the paramagnetic salt $CuSO_4$ in pure water; and a precision measurement of the ratio of the gyromagnetic ratio of F^{19} to that of H^1.

C. Proton Resonance Line Widths

In Chapter II, Section E, entitled "The RF Susceptibilities and the Saturation Phenomenon," it is brought out that the relaxation time T_2 is operationally defined as a characteristic average interval of uninterrupted precession of individual nuclei in their liquid environment. It is thus a direct modulus of the coherence of precession and therefore of the *spectrum* of frequencies which characterize the precession phenomenon. This *spectrum* reveals itself macroscopically in a real liquid sample of

Table 2. Observed absorption line width as a function of molarity. The actual widths shown are the intervals ΔB (in gauss) between maxima and minima of the derivative traces.

Molarity	Observations	ΔB (gauss)	Std. Dev.
Saturated	6	2.119	0.212
1.0 M	13	2.022	0.094
0.33 M	10	1.853	0.150
0.026 M	11	1.767	0.061

nuclei (say, protons) as simply the Lorentzian line width of the NMR signal. One of the most convenient ways to control the number of times per second the nuclei are disturbed from their orderly precession is the addition of a controlled amount of paramagnetic salt such as $CuSO_4$ into the nuclear environment. Thus, we expect from the theory that large concentrations of $CuSO_4$ in the water should give broad NMR "lines" (really Lorentzian distributions of frequencies) whereas low concentrations should give narrow lines. This explicit dependence of linewidth on T_2 is shown in detail in equation (49) of Chapter II. (The Cu^{++} ion provides the electromagnetic disturbance required to interrupt the precession.)

This motivation of the theoretical background of line width versus paramagnetic salt concentration led to the experimental results presented in Table 2.

The experimental technique used to calibrate the sweep in gauss/cm to yield line widths in gauss is illustrated in Figure 18. Two proton resonances from the same sample are carefully displaced from each other on one baseline (ramp). The frequency (f) of the oscillator for each resonance is measured to five significant figures, and then the linear scale in gauss/cm results from the application of $f = \gamma B$ (see equation (23)) to yield $f_2 - f_1 = \gamma(B_2 - B_1)$. Since f_1, f_2, and γ are known, $B_2 - B_1$ as measured between the zero-crossing points of the two resonances immediately gives the desired calibration. A mean of 0.6375 ± 0.0137 gauss/cm was obtained for six observations.

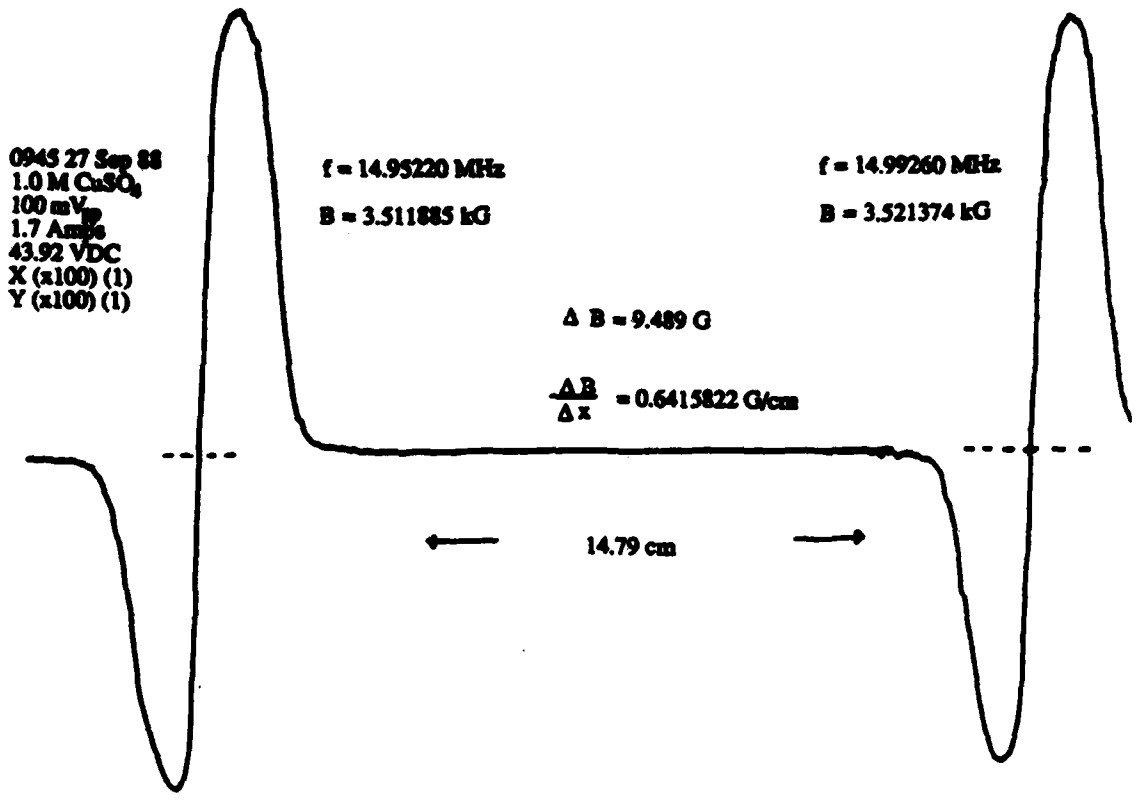

Figure 18. Sample calibration plot.

Then a line width of a particular derivative signal is the $\triangle B$ measured between the upper and lower peaks of the trace on the X-Y recorder. (See Figure 19.)

The change in line width with varying concentration of $CuSO_4$ as displayed in Table 2 is monotonic within the indicated error as expected. However, the sensitivity of line width to change of $CuSO_4$ concentration is not remarkable. This lack of sensitivity is attributed to inhomogeneity of the magnetic field of the student laboratory magnet used. As is shown in Chapter II, page 13, the observed line width is always contaminated at least to some extent by variation of the magnetic field within the volume of any NMR sample. Specifically

$$\frac{1}{T_2^*} = \frac{1}{T_2} + \frac{1}{\gamma \triangle B} \quad .$$

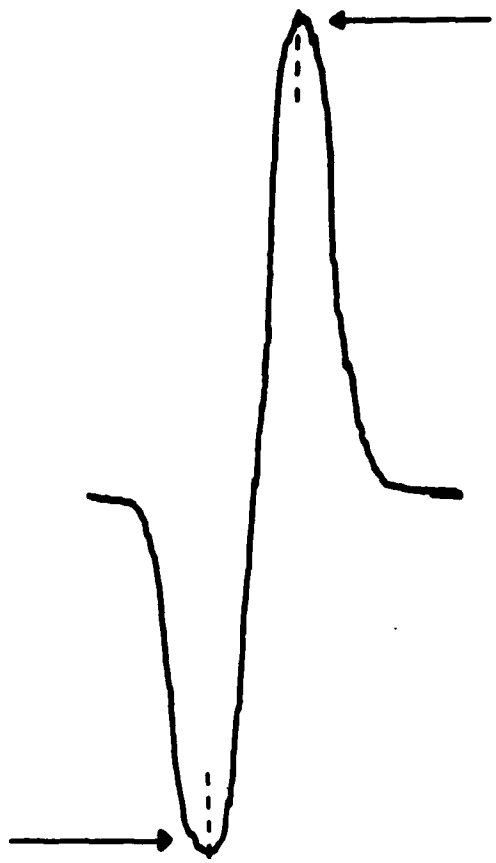

Figure 19. Representative line width plot.

in which T_2^* is inversely proportional to the observed line width, T_2 is the intrinsic transverse relaxation time, and $\gamma \triangle B$ is the *fixed* contribution of field inhomogeneity to the observed line width. (The factor $\triangle B$ is simply some convenient measure of this inhomogeneity.) Since $1/\gamma \triangle B$ is a constant instrumental contaminant, changes in T_2^* can be obscured considerably as T_2 changes over a wide range.

D. Gyromagnetic Ratio Measurements

The frequency of the fluorine (F^{19}) resonance in trifluorobenzene immersed in a fixed $\vec{B}$-field was accurately compared with the frequency of the proton resonance using the same sample in precisely the same field. The frequencies can be measured

in this experiment routinely to 1 part in 7.0×10^5. Since $f = \gamma B$, with fixed B the ratio γ_f/γ_p is measurable in principle to a precision of 2 parts in 7.0×10^5.

The actual procedure used in this experiment gave results with less than the possible precision as will now be explained. First the prominent proton resonance in trifluorobenzene was found and identified by comparison with auxiliary pure proton samples using the hybrid Darlington marginal oscillator. Then the magnetic field was increased in search of the fluorine resonance. In spite of our knowledge of approximately where the fluorine signal should occur, hours of searching were frustratingly unsuccessful. It was at this point that the suspicion that a *narrow* fluorine line (long T_2) was being heavily saturated by an RF level which did *not* saturate the proton line and thus allowed the proton signal to show up readily. In order to reduce the RF level in the marginal oscillator tank to try to avoid this saturation, the idea arose to inject RF at a very low level into the tank circuit from a frequency synthesizer. The feedback control in the marginal oscillator was set at a point below the level of self-sustained oscillation. Then the injection of external RF power very loosely coupled to the RF tank coil sustained a controllable and much reduced level of oscillation of the marginal oscillator, as has been explained in the section describing the *injection system* in Chapter III. In this experimental environment the fluorine line, now *not* saturated, showed up immediately. The procedure then pursued was to carefully adjust the fluorine line to the center of the ramp and record the frequency of the marginal oscillator. Next, with the $\vec{B}$-field fixed at its new, higher value, the frequency of the marginal oscillator was increased slowly until the prominent proton resonance was centered on the ramp. Recording of this second frequency (the proton frequency) completed the data required to give the ratio of the fluorine gyromagnetic ratio to that of the proton. This procedure was repeated seven times. The data are shown in Table 3. The resulting average of 0.9409 ± 0.0007 is a tribute to this procedure which depends only on precise frequency measurements and the ability to judge

Table 3. Ratio of the fluorine gyromagnetic ratio to that of the proton.

Trial no.	γ_f/γ_p (exp.)	γ_f/γ_p (act.)	$\Delta\%$
1	0.9422	0.9408	0.1486
2	0.9409	0.9408	0.0106
3	0.9405	0.9408	0.0319
4	0.9410	0.9408	0.0213
5	0.9397	0.9408	0.1171
6	0.9410	0.9408	0.0213
7	0.9411	0.9408	0.0319

when a signal is close to the center of the ramp. This latter somewhat subjective manipulation is the only factor which prevents a precision of 2 parts in 7.0×10^5.

Since this experiment using the novel injection method was so successful with the hybrid Darlington marginal oscillator, the question naturally arose whether the modified Donnally circuit would perform well in this mode. The modified Donnally oscillator was simply substituted in the gyromagnetic ratio experiment and was found to work surprisingly well. All tests of this injection mode appeared to indicate, in fact, that the modified Donnally oscillator was somewhat more sensitive than the hybrid Darlington in producing easily observable fluorine as well as proton signals. The only disadvantage of using the Donnally circuit was the necessity for continual adjustment of marginality to maintain the optimum signal. No such readjustment was ever necessary in the use of the hybrid Darlington in this experiment. A decision was made on this basis not to repeat the gyromagnetic ratio experiment with the Donnally circuit.

CHAPTER V

CONCLUSION

It has been demonstrated that a conceptually uncomplicated nuclear magnetic resonance marginal oscillator spectrometer with good performance characteristics can be assembled with inexpensive components. An accurate comparison of signal-to-noise capabilities of three different marginal oscillators led to the selection of a hybrid Darlington circuit for the performance of two experiments: proton line width measurements and a precision comparison of the F^{19} gyromagnetic ratio to that of the proton. Of the other two marginal oscillators, only the modified Donnally circuit came close to favorable comparison with the hybrid Darlington. The third oscillator, the FET cascade circuit, was a disappointing third in the rankings for reasons that are yet to be understood and was summarily eliminated from further consideration in this work.

In addition to the original design of the hybrid Darlington marginal oscillator, two special and novel features of the spectrometer system developed are: a sensitive and easy to understand phase sensitive detector; and a new injection mode of marginal oscillator operation which provides low RF fields for observation of easily saturated NMR lines.

REFERENCES

1 B.V. Rollins, *Nature*, vol. 158, p. 669, 1946.

2 R.V. Pound and W.D. Knight, *Rev. Sci. Instrum.*, vol. 21, p. 219, 1950.

3 R.N.H. Robinson, *J. Sci. Instrum.*, vol. 36, p. 481, 1959.

4 E.M. Purcell, H.C. Torrey, and R.V. Pound, *Physical Rev.*, vol. 69, p. 37, 1946.

5 P. Grivet, M. Soutif, and R. Gabillard, *Physica*, vol. 17, p. 420, 1951.

6 J. Larmor, *Mathematical and Physical Papers*. Cambridge, England: University Press, 1929.

7 F. Bloch, *Physical Rev.*, vol. 70, p. 420, 1951.

8 L. Boltzmann, *Lectures on Gas Theory*. Berkeley, CA: University of California Press, 1964.

9 A. Abragam, *The Principles of Nuclear Magnetic Resonance*. Oxford, England: University Press, 1967.

10 N. Bloembergen, *Nuclear Magnetic Relaxation*. New York: W.A. Benjamin Incorporated, 1961.

11 G.E. Pake, *Am. J. Physics*, vol. 18, p. 438, 1950.

12 E. Fukushima and S.B.W. Roeder, *Experimental Pulse NMR: A Nuts and Bolts Approach*. Reading, MA: Addison Wesley, 1981.

13 B. Donnally and T.M. Sanders, *Rev. Sci. Instrum.*, vol. 31, p. 978, 1960.

SUPPLEMENTARY SOURCES CONSULTED

1 T.L. Flugum, "Nuclear Magnetic Absorption Line Widths in Weak Magnetic Fields with a Robinson Oscillator," Masters thesis, Texas A&M University, August, 1987, unpublished.

2 W. Franzen, *Rev. Sci. Instrum.*, vol. 33, pp. 933-938, 1962.

3 . M.W. Garrett, *J. Appl. Phys.*, vol. 22, p. 1091, 1951.

4 E.L. Hahn, *Physical Rev.*, vol. 70, p. 145, 1949.

5 J.K. Hardy, *High Frequency Circuit Design*. Reston, VA: Reston Pub. Co., 1979.

6 P. Horowitz and W. Hill, *The Art of Electronics*. Cambridge, England: Cambridge University Press, 1987.

7 K. Kaminishi and S. Nawata, *Rev. Sci. Instrum.*, vol. 52, p. 447, 1981.

VITA

Frank Phillip Willingham was born in Jasper, Alabama on 28 September 1956 to James E. and Gladys E. Willingham. He graduated from Walker High School in May 1974, Georgia Military College (A.S.) in May 1976 and The United States Military Academy (B.S., National Security and Public Affairs) in May 1980. Upon graduation from West Point, he was commissioned an infantry second lieutenant in the U. S. Army and was assigned to the 193d Infantry Brigade in The Republic of Panama. Returning to the United States in 1983, he was stationed at Fort Hood, Texas where he commanded a mechanized infantry company in the 2d Armored Division and subsequently met his lovely wife Elizabeth (Liz). Upon completion of the requirements for the degree of Master of Science in December 1988 he will be assigned as an instructor in the Department of Physics at The United States Military Academy, West Point, New York. His permanent mailing address is: 1606 East 69 Highway, Jasper, Alabama 35501.